Application of High Order Traffic Flow Models for Incident Detection and Modeling Multiclass Flow

Shimao Fan* Ren Wang† Daniel B. Work‡

August 25, 2014

Final report submitted to
the University of California, Berkeley

*Coordinated Science Laboratory, University of Illinois at Urbana Champaign, 205 N. Mathews Ave, Urbana, IL 61801 (shimao@illinois.edu)

†Department of Civil and Environmental Engineering, University of Illinois at Urbana Champaign, 205 N. Mathews Ave, Urbana, IL 61801 (renwang2@illinois.edu)

‡Department of Civil and Environmental Engineering and Coordinated Science Laboratory, University of Illinois at Urbana Champaign, 205 N. Mathews Ave, Urbana, IL 61801 (dbwork@illinois.edu)

Abstract

This work is focused on the application of high order traffic flow theory to the problem of traffic incident detection, and for modeling multiclass traffic flow composed of different vehicle types.

For incident detection applications, a class of *generic second order traffic flow models* (GOSM) is applied to detect traffic incidents in real time by posing the problem as a hybrid state estimation problem. To incorporate the incident dynamics in the model, a regime variable is introduced to describe where and how many lanes are blocked during an incident, resulting in a multiple model framework. This work develops a multiple model extension to the GOSM on a road network. Then, a discrete version of the GOSM known as the *second order cell transmission model* (2CTM) is presented under the framework of the cell transmission model. Next, this multiple model predictor is integrated with a particle filter to obtain an estimate of the traffic state and the incident location if it exists. The proposed algorithm is tested on a road segment in numerical simulation using the CORSIM traffic microsimulation software as the true state.

In the second application, a new family of high order traffic flow models is considered as an extension to the scalar *Lighthill Whitham Richards* (LWR) model. Under this framework, a heterogeneous traffic model with two vehicle classes is developed to capture an important phenomenon in highly heterogeneous traffic flows called creeping. Creeping occurs when small vehicles such as motorcycles continue to advance in congestion even though larger vehicles have completely stopped, for example via lane sharing. The new model is a phase transition model which applies a system of conservation laws in the non-creeping phase, and a scalar model in the creeping phase. The solution to the Riemann problem is obtained by investigating the elementary waves, in particular for the cases when one vehicle class is absent, as well as in the presence of a phase transition. Based on the proposed Riemann solver, the solution to the Cauchy problem is constructed using wavefront tracking. Numerical tests are carried out using a Godunov scheme to illustrate the creeping phenomenon.

Contents

List of Tables

List of Figures

1 Introduction

This work is focused on solving the following two research problems. The first objective is to develop a multiple model traffic state estimation framework based on a family of second order traffic flow models and apply it to detect traffic incidents in real time. The second objective is to design a new model for multiclass traffic flow that can capture several key features of the flow when vehicles are heterogeneous in size.

1.1 Real Time Incident Detection

The objective of traffic estimation is to monitor the traffic state. The traffic state (e.g., traffic density along the roadway) can be estimated with traffic models and nonlinear filtering techniques, where traffic models are used to predict the traffic state given the initial and boundary conditions, and the nonlinear filters are used to improve the predictions by incorporating information from real–time sensor measurements. Traffic estimation techniques have advanced rapidly in recent years because of developments in nonlinear filtering techniques, advances in sensing technologies such as GPS data from cellphones, and the availability of cheap computing and communication resources.

Most existing traffic estimation algorithms assume time–invariant parameters in the traffic model and do not account for changes in the dynamics on the highway caused by traffic incidents. While a calibrated traffic estimation model can perform well under normal traffic operating conditions, it will provide poor traffic state estimates when a traffic incident occurs, because the deterministic traffic model does not contain any dynamics to describe the traffic flow evolution under incidents. By incorporating incident dynamics into the traffic model, it is possible to jointly estimate the traffic state and detect incidents.

The work is motivated by the fact that jointly estimating incidents and the traffic state can improve both incident detection capabilities and the traffic state estimates. Clearly, knowledge of an incident can improve post–incident traffic state estimates. On the other hand, knowledge of the traffic state can be used to improve detection of incidents, by observing when the predicted traffic state differs significantly from the observed measurements. To address the problem of jointly estimating incidents and the traffic state, this work poses the problem as a hybrid system state estimation problem. It then proposes a nonlinear particle filtering technique to solve the estimation problem, using a second order traffic flow model in the filter. Finally, the performance of the filter is evaluated in numerical experiments using CORSIM.

1.2 Heterogeneous Multiclass Traffic Modeling

Modern traffic control and traffic estimation techniques increasing rely on sound traffic flow models, which are capable of capturing realistic details of traffic dynamics. Recently, traffic models that distinguish different vehicle classes have received considerable attention, and several of these models are appropriate to capture richer dynamics in multiclass traffic flow, such as *overtaking* between vehicle classes. When the traffic flow is composed of vehicles which are highly heterogeneous in size (cars, buses, motorcycles, etc.), the phenomenon called *creeping* is observable, which describes a scenario when small vehicles continue to advance in congestion even though larger vehicles have completely stopped. This phenomenon occurs in city traffic flow and highway traffic flow in congestion. For instance, small vehicles such as motorcycles can move to the front of the queue as they are approaching to a red traffic light via lane sharing.

In this study, we develop a heterogeneous multiclass traffic model under a framework of high order traffic flow models that has several important features: (*i*) it allows creeping, which permits small vehicles to move, even when large vehicles have completely stopped; (*ii*) it is *anistropic*, where information cannot travel faster than the fastest vehicle class; (*iii*) it is consistent with the LWR model when only one vehicle class is present; (*iv*) it is well-posed away from the *vacuum*, i.e., the point where both vehicle classes disappear.

Well-posedness is an important property that has not been established for many heterogeneous models. The models that assign a unique maximum traffic velocity to each vehicle class [3, 52] have non-vacuum *umbilic points* where strict hyperbolicity is lost [3, 55]. Hence, they do not fit the standard conservation laws theory (e.g., [8, 31, 32]), which leads to a challenge in proving the well-posedness of the system. This work presents a different way to distinguish velocity functions that enables creeping and moves the umbilic point to the vacuum. This simplifies the mathematical analysis considerably, and allows for a well-posed system away from the vacuum.

1.3 Contributions and Outline

The main contributions of this work are as follows. This work solves the joint traffic state estimation and incident detection problem by applying a second order traffic flow model within a particle filtering framework. Specifically, the second order traffic flow model is implemented with a multiple model particle filter algorithm to solve the joint traffic state estimation and incident detection problem by using incident data simulated by a microscopic traffic simulation software CORSIM.

The main contributions of the multiclass traffic modeling work involves three aspects: (*i*) it is first shown that a family of second order models (GOSM) is equivalent to a two class homogeneous multiclass model, which completes the mathematical analysis associated with these models, and justifies that the GOSM is not suitable to model creeping; (*ii*) a new two class heterogeneous model that allows creeping is introduced; and (*iii*) a comprehensive investigation of the properties of the new model is provided.

The remainder of this report is organized as follows. In Section 2.1, a class of second order models called *generic second order model* (GOSM) is introduced, and a second order generalization of the cell transmission model is proposed based on a discretized version of the GOSM, called the 2CTM. The 2CTM is presented by analyzing the sending and receiving of traffic flow, which acts as a model predictor in the forward estimation problem. A multiple model framework based on the 2CTM is proposed by introducing a regime variable to indicate the number of the open lanes on the freeway in Section 2.2. Section 2.3 is devoted to introduce the technique to solve the network problem when the GOSM is applied. In this process, a single road junction problem is studied in detail for three common types of road junctions (*bottlenecks, merges*, and *diverges*), and a model predictor on a road network under the multiple model framework is presented. Next, a hybrid state estimation problem is introduced by applying a particle filter to the model in Section 2.4. The simulation results based on the software CORSIM are presented and a discussion of the results is provided in Section 2.5.

In Section 3.1, a connection between the GOSM and the homogeneous two class models is introduced. Based on properties of homogeneous multiclass models, the GOSM is not appropriate to model creeping. A new heterogeneous model for two vehicle classes is proposed and its properties are outlined in Section 3.2. The mathematical analysis of the model is presented in Section 3.3, which includes verifying the model is strictly hyperbolic away from the vacuum, investigating the elementary waves and using them to construct a Riemann solver, and providing a sketch of the proof of the well-posedness of the model. Section 3.4 is devoted to validate the features of the proposed model by performing numerical simulations and comparing to the n–populations model [3].

2 Joint Traffic State Estimation and Incident Detection

In this work, the joint traffic state estimation and incident detection problem is posed as a hybrid state estimation problem using the following evaluation–observation system:

$$\begin{aligned} u^{k+1} &= \mathcal{F}\left(u^k, \mu^{k+1}\right) + \eta^k, \\ z^{k+1} &= h^{k+1}\left(u^{k+1}, \mu^{k+1}\right) + \nu^{k+1}, \end{aligned} \tag{1}$$

where $u^k = \begin{pmatrix} \rho^k \\ y^k = \rho^k w^k \end{pmatrix}$ is the traffic state at time $t = k\Delta t$, where Δt is the discrete timestep. Here, ρ^k and w^k represent the traffic density and the *property* of vehicles, respectively. Moreover, $y^k = \rho^k w^k$ defines the *total property*. In an incident detection problem, a discrete regime variable μ that identifies the location, severity, and duration of an incident is introduced. Here, μ depends on both time and space, i.e., $\mu(x,t)$. In the discrete domain,

μ^k represents the number of lanes that are open during $(k\Delta t, (k+1)\Delta t]$. Moreover, η^k is the prediction error, and ν^{k+1} represents the measurement error.

Given the evolution observation system (1), the traffic estimation and incident detection problem can be posed as the problem of estimating the traffic state u^k and the model μ^k given measurements $\{z^1, \cdots, z^k\}$. This problem is hard to solve for the following reasons. First, the traffic model is nonlinear and switches between models due to the incident variable μ. Second, traffic measurements are usually not available for the entire space domain. For instance, when a traffic incident occurs between two sensors, the algorithm is not able to detect the incident in real time since the incident information takes time to propagate to a sensor where it can be detected. When the incident information propagates to a sensor, it is also hard for the estimation algorithm to correctly track the traffic state, because it is not always possible to uniquely determine if and where the incident occured.

In the next section, we first describe the traffic model used for traffic prediction. In particular, the method to develop a model predictor $\mathcal{F}(\cdot)$ for a family of second order models on road network is introduced.

2.1 Second Order Traffic Model

2.1.1 Generic Framework of Second Order Models

A family of macroscopic models that fit into the framework of the GSOM [34] are considered:

$$\begin{aligned} \rho_t + (\rho v)_x &= 0, \\ w_t + v w_x &= 0, \\ \text{with} \quad v &= V(\rho, w), \end{aligned} \tag{2}$$

where $\rho(x,t)$ and $v(x,t)$ represent the traffic density and traffic velocity, respectively. Both variables depend on both space x and time t. The first equation of (2) describes the conservation of vehicles. The second equation of (2) indicates that w is advected with vehicles at the speed of traffic flow v, and thus w represents a *property* of vehicles. Moreover, the velocity function $V(\rho, w)$ is strictly decreasing in the density, i.e., $\frac{\partial V}{\partial \rho} < 0$. The quantity w is used to relate driver properties to the flow–density curves. Thus, the GSOM possesses a family of flow–density curves parametrized by w, i.e., $Q(\rho, w) = \rho V(\rho, w)$ (see Figure 1).

For convenience, the conservation form of (2) is considered:

$$\begin{aligned} \rho_t + (\rho v)_x &= 0, \\ y_t + (yv)_x &= 0, \\ \text{with} \quad y = \rho w, \quad v &= V(\rho, y/\rho), \end{aligned} \tag{3}$$

where the conserved quantity y is a *momentum* [2, 12], which is originally motivated from gas dynamics, but lacks physical interpretation. Since w is advected with vehicle flows, ρ is conserved and so is $y = \rho w$.

Note that it is important to give y a clear physical meaning to properly design a discrete *cell transmission model* [14] (CTM) equivalent for (3). A suitable definition for $y = \rho w$ is to recognize that it is a *total property*, where the property w may have various meanings, such as "aggressivity" [17], "desired spacing" [56], or "perturbations" [6]. Thus, the second conservation equation of (3) expresses the conservation of the total property. For example, imaging the property w as the average number of passengers carried by each vehicle, it is clear that the total passengers is conserved on a road segment.

Another example for the definition of the property quantity is to define w as the fraction of one vehicle class. As shown later, by defining w as the fraction of cars for a multiclass flow that is composed of cars ($j = 1$) and trucks ($j = 2$), i.e., $w = \rho_1/\rho$, where $\rho = (\rho_1 + \rho_2)$ is the total traffic density, the GOSM is equivalent to a two class multiclass traffic flow model.

2.1.2 Classification of the GOSM

The macroscopic traffic models that fit into the GSOM framework (2) is classified based on the assumptions on the property quantity w. When all drivers have the same property, the

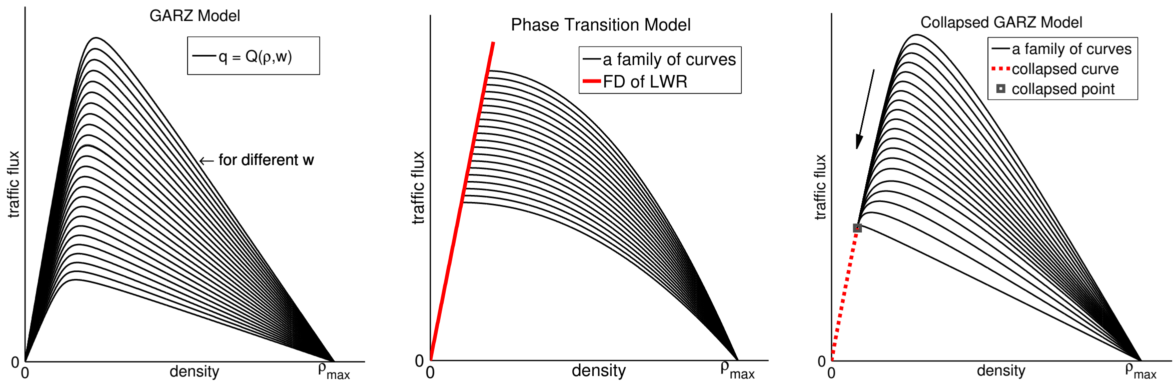

(a) (b) (c)

Figure 1: *(a) flow–density curves of the GARZ model [17]. (b) flow–density curves of a phase transition model. (c) illustrates the idea of collapsed model [18].*

GSOM collapses to the *Lighthill–Whitham–Richards* model (LWR) [38, 46]:

$$\rho_t + (\rho V(\rho))_x = 0, \tag{4}$$

where the velocity depends only on the density. The unique flow–density relationship $Q(\rho) = \rho V(\rho)$ defines a *fundamental diagram* (FD). Hence, the LWR model is a simplified form of the GSOM by assigning a uniform property $w(x,t) = \bar{w}$ [19], i.e., $V(\rho) = V(\rho, \bar{w})$. The LWR model can be discretized resulting in the cell transmission model [14], which is consistent with the well known Godunov scheme [22], as shown by Lebacque [33].

The model proposed by *Aw and Rascle* [2] and *Zhang* [53] (ARZ) and the *generalized Aw–Rascle–Zhang model* (GARZ) [17] allow drivers to possess different properties. For instance, in [53], the velocity function is defined as:

$$V(\rho, w) = V_{\mathrm{eq}}(\rho) + (w - V_{\mathrm{eq}}(0)), \tag{5}$$

where $V_{\mathrm{eq}}(\rho)$ represents the *equilibrium velocity function*. The associated flow–density function $Q_{\mathrm{eq}}(\rho) = \rho V_{\mathrm{eq}}(\rho)$ is an *equilibrium fundamental diagram*. From (5), a family of velocity curves is generated by shifting the equilibrium velocity curve vertically with $V(0, w) = w$.

One sees that $\frac{\partial V}{\partial w} = 1 > 0$, which means that the traffic velocity always depends on w for $\rho \in [0, \rho_{\max}]$, where $\rho_{\max}$ is the maximum traffic density. Similarly, one also has $\frac{\partial V}{\partial w} > 0$ for $\rho \in [0, \rho_{\max}]$ in the GARZ model. As a result, the flow–density curves of the ARZ and GARZ models are distinct even in freeflow (away from the *vacuum*, i.e., $\rho = 0$), (see Figure 1(a)). Thus, these models are not appropriate to capture distinct behaviors in the freeflow and congested regimes based on empirical observation by Kerner [28, 29], who observed that the experimental flow data is positively proportional to the density data in freeflow, while the flow–density data exhibits large spread in congestion.

For the *collapsed generalized ARZ model* (CGARZ) [18], it is assumed that the difference in property does not affect the traffic velocity in freeflow. This means that vehicles always possess different properties, but the traffic velocity is not affected by w in freeflow, i.e., $\frac{\partial V}{\partial w} = 0$. The CGARZ model is a special form of the GARZ model that collapses the flow–density curves into a single curve in the freeflow region (see Figure 1(c)). As a result, all the analytical results of the ARZ and the GARZ models [2, 17, 34] transfer over to the CGARZ model. Furthermore, the CGARZ model successfully captures distinct behaviors of traffic flow in the freeflow and congested regions.

Based on the assumption on w, one sees an important distinction between *phase transition models* [5, 6, 12, 13] and the GOSM. In phase transition models, an LWR model is applied in the freeflow phase Ω_{f}, and a second order model is employed in the congested phase Ω_{c} (see Figure 1(b)). Hence, phase transition models assume a uniform property w in Ω_{f}, but allow for different properties in Ω_{c}. These models admit phase transitions in traffic flow, which agrees with Kerner's empirical observation [28, 29]. However, by fixing w in freeflow, a phase transition model uses the philosophy that vehicles lose their properties in Ω_{f}. In contrast, the GOSM assumes that drivers always preserve their properties, independent of the congestion level.

One sees that the CGARZ model [18] combines the good features of both phase transition models [5, 6, 12, 13] and the GARZ model [17], while it also avoids the complicated analytical work in a phase transition model. It is also appropriate to model distinct behaviors in freeflow

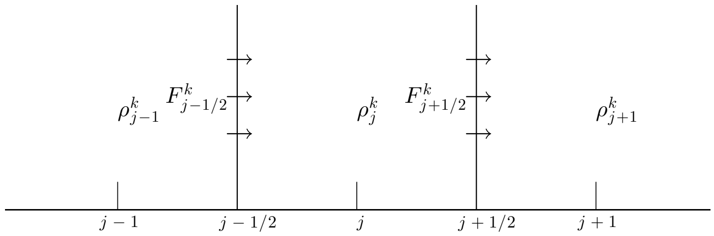

Figure 2: *The cell transmission model.*

and congested phases based on Kerner's theory [28, 29]. For the simulations performed in this study, the CGARZ model is applied. Next, a discrete formulation of the GOSM (3) is developed under the CTM framework.

2.2 Multiple Model Second Order Cell Transmission Model

The multiple model framework is based on the fact that traffic model changes in the presence of an incident. In this section, a *second order cell transmission model* (2CTM) without an incident is presented first. Then, a multiple model framework based on the 2CTM is developed by involving the regime variable μ, which denotes the number of lanes that is open.

Mostly due to the complexity of the mathematical analysis, and the difficulty to obtain physical interpretations in the construction of solutions for the GOSM (3) (e.g., the existence of an *intermediate state* in the Riemann solver [2, 12]), it is desirable to reformulate the GOSM (3) in a more intuitive way such as the CTM. In [35], a Riemann solver to the GOSM is constructed by examining the sending and receiving functions for traffic, which is consistent with the original solver that is based on analyzing elementary waves (see e.g., [2, 53]). This equivalence makes it possible to construct the 2CTM by analyzing the potential to send vehicles from the upstream cell and receive vehicles from the downstream cell.

2.2.1 Cell Transmission Model

First, the features of the CTM are summarized. Recall that the CTM [14] is based on the integral form of the LWR model (4):

$$\frac{d}{dt}\int_a^b \rho(x,t)dx = q(a,t) - q(b,t),$$

where $q(a,t)$ and $q(b,t)$ represent the incoming and outgoing fluxes at the boundaries of a cell, and the integral on the left is the number of vehicles on the road segment $x \in [a,b]$.

The CTM discretizes space into cells with size Δx, and studies each cell by examining its inflow and outflow over the time interval Δt. We consider three adjacent cells $(j-1,\, j,\, j+1)$ with initial densities ρ_{j-1}^k, ρ_j^k, and ρ_{j+1}^k at the time $t = k\Delta t$, and study the evolution of traffic density in the jth cell (see Figure 2). The key features of the CTM are listed as follows.

1. The evolution equation is given by the Godunov method [22]:

$$\rho_j^{k+1} = \rho_j^k + \frac{\Delta t}{\Delta x}\left(F_{j-1/2}^k - F_{j+1/2}^k\right), \tag{6}$$

   where $F_{j-1/2}^k$ and $F_{j+1/2}^k$ are the inflow and outflow of the jth cell.

2. $F_{j-1/2}^k$ and $F_{j+1/2}^k$ are determined by the minimum of the vehicles available to be sent from the upstream, and the availability of the downstream cell to receive vehicles:

$$F_{j-1/2}^k = \min\left\{S\left(\rho_{j-1}^k\right), R\left(\rho_j^k\right)\right\}, \qquad F_{j+1/2}^k = \min\left\{S\left(\rho_j^k\right), R\left(\rho_{j+1}^k\right)\right\},$$

   where $S(\cdot)$ and $R(\cdot)$ are the sending and receiving functions.

3. The sending and receiving functions are defined based on $Q(\rho)$:

$$S(\rho) = \begin{cases} Q(\rho), & \text{if } \rho \le \rho_c, \\ Q_{\max}, & \text{if } \rho > \rho_c, \end{cases} \qquad R(\rho) = \begin{cases} Q_{\max}, & \text{if } \rho \le \rho_c, \\ Q(\rho), & \text{if } \rho > \rho_c, \end{cases} \tag{7}$$

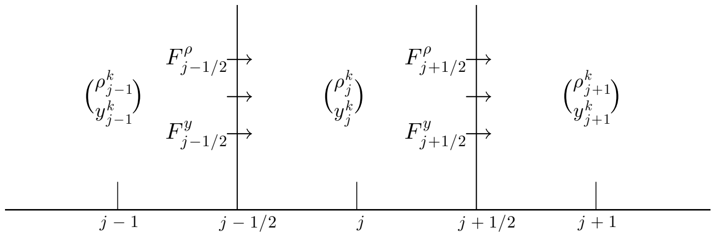

Figure 3: *Second order cell transmission model.*

where ρ_c denotes the critical density where the maximum traffic flow $Q_{\max}$ is obtained.

2.2.2 Second Order Cell Transmission Model

The 2CTM is designed based on a Godunov discretization of the GOSM (3). For a system of conservation laws (3), the initial traffic states in three adjacent cells ($j-1$, j, $j+1$) are vectors $u^k_{j-1} = \left(\rho^k_{j-1}, \rho^k_{j-1}w^k_{j-1}\right)$, $u^k_j = \left(\rho^k_j, \rho^k_j w^k_j\right)$, and $u^k_{j+1} = \left(\rho^k_{j+1}, \rho^k_{j+1}w^k_{j+1}\right)$ at the time $t = k\Delta t$ (see Figure 3). By applying the Godunov scheme [22, 36] to (3), the 2CTM has the following form:

$$\begin{aligned} \rho^{k+1}_j &= \rho^k_j + \frac{\Delta t}{\Delta x}\left(F^{\rho}_{j-1/2} - F^{\rho}_{j+1/2}\right), \\ y^{k+1}_j &= y^k_j + \frac{\Delta t}{\Delta x}\left(F^{y}_{j-1/2} - F^{y}_{j+1/2}\right), \end{aligned} \tag{8}$$

which provides evolution equations for both conserved quantities, the traffic density ρ and total property $y = \rho w$. Here, F^{ρ} and F^{y} are the flows of ρ and y, respectively.

To determine F^{ρ} and F^{y}, it is important to note that these two kinds of flow are related. Since the property w is always advected with vehicle flow F^{ρ}, the flow of total property F^{y} is computed by multiplying the average property w of the upstream vehicles (with respect to the cell boundary) to the flow of vehicles:

$$F^{y}_{j-1/2} = w^k_{j-1}F^{\rho}_{j-1/2}, \qquad F^{y}_{j+1/2} = w^k_j F^{\rho}_{j+1/2},$$

where w^k_{j-1} and w^k_j are the properties of vehicles at the cells $j-1$ and j, and $F^{\rho}_{j-1/2}$ and $F^{\rho}_{j+1/2}$ are the associated traffic fluxes across the cell boundaries. Thus, the update equations

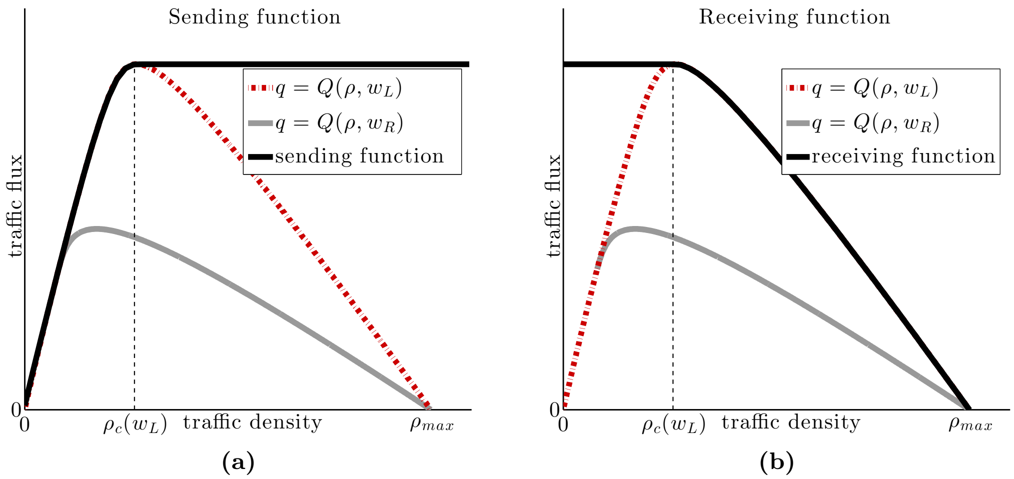

Figure 4: *(a) is the sending function and (b) is the receiving function of the 2CTM based on the CGARZ model [18], illustrated for the case where $w_L > w_R$.*

(8) simplify to

$$\begin{aligned} \rho_j^{k+1} &= \rho_j^k + \frac{\Delta t}{\Delta x}\left(F^{\rho}_{j-1/2} - F^{\rho}_{j+1/2}\right), \\ y_j^{k+1} &= y_j^k + \frac{\Delta t}{\Delta x}\left(w^k_{j-1}F^{\rho}_{j-1/2} - w^k_j F^{\rho}_{j+1/2}\right). \end{aligned} \tag{9}$$

Next, the vehicle flow through a cell boundary is the minimum of the sending and receiving functions, as in the CTM. To complete the scheme (9), it is sufficient to define the sending and receiving functions for ρ, as in the CTM.

Remark 1. By assuming that all vehicles have the same property as the LWR model, i.e., $w = \bar{w}$, the update equation for y is identical to that for ρ, since it becomes

$$\bar{w}\rho_j^{k+1} = \bar{w}\rho_j^k + \frac{\Delta t}{\Delta x}\left(\bar{w}F^{\rho}_{j-1/2} - \bar{w}F^{\rho}_{j+1/2}\right),$$

where $\bar{w}$ can be canceled out. Thus, the 2CTM is consistent with the classical CTM (6) when the property quantity is fixed.

2.2.3 Sending and Receiving Functions of 2CTM

Let $u_{\mathrm{L}} = (\rho_{\mathrm{L}}, \rho_{\mathrm{L}} w_{\mathrm{L}})$ and $u_{\mathrm{R}} = (\rho_{\mathrm{R}}, \rho_{\mathrm{R}} w_{\mathrm{R}})$ be the traffic states of the upstream and downstream cells, the sending and receiving functions for the GSOM are proposed in [35] (see Figure 4):

$$S(\rho_{\mathrm{L}}, w_{\mathrm{L}}) = \begin{cases} \rho_{\mathrm{L}} v_{\mathrm{L}}, & \text{if } \rho_{\mathrm{L}} \le \rho_{\mathrm{c}}(w_{\mathrm{L}}), \\ Q_{\max}^{w_{\mathrm{L}}}, & \text{if } \rho_{\mathrm{L}} > \rho_{\mathrm{c}}(w_{\mathrm{L}}), \end{cases} \qquad R(\rho_{\mathrm{M}}, w_{\mathrm{L}}) = \begin{cases} Q_{\max}^{w_{\mathrm{L}}}, & \text{if } \rho_{\mathrm{M}} \le \rho_{\mathrm{c}}(w_{\mathrm{L}}), \\ \rho_{\mathrm{M}} v_{\mathrm{M}}, & \text{if } \rho_{\mathrm{M}} > \rho_{\mathrm{c}}(w_{\mathrm{L}}), \end{cases} \tag{10}$$

where $v_{\mathrm{L}} = V(\rho_{\mathrm{L}}, w_{\mathrm{L}})$ is the traffic velocity of the upstream vehicles, and $Q_{\max}^{w_{\mathrm{L}}}$ is the maximum traffic flow based on $Q(\rho, w_{\mathrm{L}})$, and $\rho_{\mathrm{c}}(w_{\mathrm{L}})$ represents the corresponding critical density. Here, the receiving function depends on an intermediate traffic state $u_{\mathrm{M}} = (\rho_{\mathrm{M}}, \rho_{\mathrm{M}} w_{\mathrm{M}})$ [2, 31], which can be calculated as:

$$\begin{cases} w_{\mathrm{M}} = w_{\mathrm{L}}, \\ v_{\mathrm{M}} \le v_{\mathrm{R}}, \quad \text{s.t.} \quad \min_{\rho} \{v_{\mathrm{R}} - v_{\mathrm{M}}(\rho)\}, \quad v_{\mathrm{M}}(\rho) = V(\rho, w_{\mathrm{M}}) \\ \rho_{\mathrm{M}}, \quad \text{s.t.} \quad v_{\mathrm{M}} = V(\rho_{\mathrm{M}}, w_{\mathrm{M}}), \end{cases} \tag{11}$$

where $v_{\mathrm{R}} = V(\rho_{\mathrm{R}}, w_{\mathrm{R}})$ is the traffic velocity of the downstream vehicles. Alternatively, the middle state ρ_M can be computed as:

$$\rho_M = \operatorname{argmin}_{\rho} \{V(\rho_R, w_R) - V(\rho, w_L)\}.$$

Note that in the case that upstream vehicles cannot match the downstream speed, i.e., the maximum possible velocity of upstream velocity is less than v_{R}, $\max_{\rho}\{V(\rho, w_{\mathrm{L}})\} = V(0, w_{\mathrm{L}}) < v_{\mathrm{R}}$, we let $v_{\mathrm{M}} = V(0, w_{\mathrm{L}})$. Otherwise, we always have $v_{\mathrm{M}} = v_{\mathrm{R}}$ (see Figure 5).

Thus, the solver (11) is rewritten as:

$$\begin{cases} w_{\mathrm{M}} = w_{\mathrm{L}}, \\ v_{\mathrm{M}} = V(0, w_{\mathrm{L}}), \quad \text{if} \quad V(0, w_{\mathrm{L}}) < v_{\mathrm{R}}, \\ v_{\mathrm{M}} = v_{\mathrm{R}}, \quad \text{otherwise}, \\ \rho_{\mathrm{M}}, \quad \text{s.t.} \quad v_{\mathrm{M}} = V(\rho_{\mathrm{M}}, w_{\mathrm{M}}). \end{cases} \tag{12}$$

The intuition behind this solver for the intermediate state is explained in more detail in the next section.

From (10) and (12), the inflow of the jth cell is computed as:

$$F^{\rho}_{j-1/2} = \min\left\{ S\left(\rho^k_{j-1}, w^k_{j-1}\right), R\left(\rho^k_{j-1/2}, w^k_{j-1}\right)\right\}, \tag{13}$$

where $\rho^k_{j-1/2}$ represents the intermediate density calculated from (12) given initial states u^k_{j-1} and u^k_j. The outflow of the jth cell can be defined in the same way. The 2CTM is summarized in Algorithm 1.

By comparing with the sending and receiving functions of the CTM (7), one notes that (i) the sending function (10) depends only on the upstream traffic state u_{L}, which is consistent with the CTM; (ii) the receiving function depends on the intermediate density ρ_{M} (which itself depends on the downstream speed v_R and upstream property w_L), and the upstream property w_{L}. It remains to provide a justification of the existence of the intermediate state and an explanation of the dependence on the upstream property. These points are explored in the next section.

2.2.4 Intermediate Traffic State

The existence of an intermediate state u_{M} in the GSOM (3) can be understood as a consequence of the interactions of vehicles with different properties w. Here, two adjacent cells (an upstream cell and a downstream cell) with initial states u_{L} and u_{R} are studied. The traffic flow through the cell interface is determined by the following rules:

Algorithm 1 *Second Order Cell Transmission Model*

Current Time Step ($t = k\Delta t$): initial traffic states in cells $j-1$, j, and $j+1$: $u_{j-1}^k = \left(\rho_{j-1}^k, \rho_{j-1}^k w_{j-1}^k\right)$, $u_j^k = \left(\rho_j^k, \rho_j^k w_j^k\right)$, and $u_{j+1}^k = \left(\rho_{j+1}^k, \rho_{j+1}^k w_{j+1}^k\right)$.

Intermediate State: Calculate the intermediate densities $\rho_{j-1/2}^k$ (between u_{j-1}^k and u_j^k) and $\rho_{j+1/2}^k$ (between u_j^k and u_{j+1}^k) from (12):

$$\rho_{j-1/2}^k = \operatorname{argmin}_\rho \left\{ V\left(\rho_j^k, w_j^k\right) - V\left(\rho, w_{j-1}^k\right) \right\},$$
$$\rho_{j+1/2}^k = \operatorname{argmin}_\rho \left\{ V\left(\rho_{j+1}^k, w_{j+1}^k\right) - V\left(\rho, w_j^k\right) \right\}.$$

Inflow and Outflow: the inflow and outflow of the jth cell are computed using (10) and (13):

$$F_{j-1/2}^\rho = \min \left\{ S\left(\rho_{j-1}^k, w_{j-1}^k\right), R\left(\rho_{j-1/2}^k, w_{j-1}^k\right) \right\},$$
$$F_{j+1/2}^\rho = \min \left\{ S\left(\rho_j^k, w_j^k\right), R\left(\rho_{j+1/2}^k, w_j^k\right) \right\}.$$

Next Time Step ($t = (k+1)\Delta t$): the traffic density and the total property $y = \rho w$ are updated to the next time step:

$$\rho_j^{k+1} = \rho_j^k + \frac{\Delta t}{\Delta x}\left(F_{j-1/2}^\rho - F_{j+1/2}^\rho\right), \quad y_j^{k+1} = y_j^k + \frac{\Delta t}{\Delta x}\left(w_{j-1}^k F_{j-1/2}^\rho - w_j^k F_{j+1/2}^\rho\right).$$

Finally, the property is obtained as $w_j^{k+1} = y_j^{k+1}/\rho_j^{k+1}$.

1. Downstream vehicles move out of way, which creates spaces for the upstream vehicles. Vehicles never move backwards.

2. Upstream vehicles maintain their property when moving from one cell to another. As a result, $w_{\mathrm{M}} = w_{\mathrm{L}}$.

3. Vehicles from the upstream cell drive as fast as possible, but not faster than the downstream vehicles. This means that $v_{\mathrm{M}} = v_{\mathrm{R}}$ whenever possible. Otherwise, v_{M} is chosen such that the gap between the velocities is minimized, i.e., $\min_\rho \{v_{\mathrm{R}} - v_{\mathrm{M}}(\rho)\}$, where $v_{\mathrm{M}}(\rho) = V(\rho, w_{\mathrm{M}})$. Note v_R depends on the downstream density and downstream property, i.e., $v_R = V(\rho_R, w_R)$.

4. Vehicles that flow through the cell interface with the property w_{L} adjust their spacing (density) to arrive the velocity v_{M} determined from rule (3), which creates an interme-

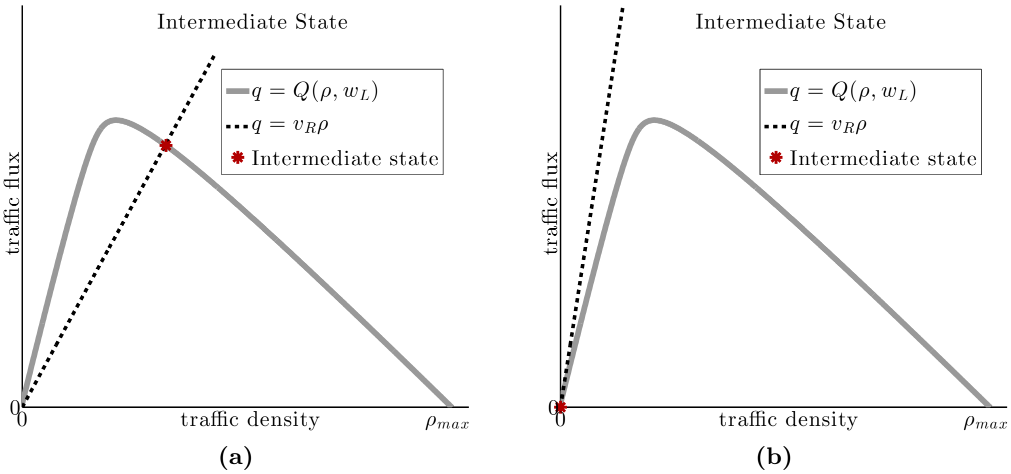

Figure 5: *(a): upstream vehicles have the potential to match the downstream velocity, i.e.,* $v_R \leq V(0, w_L)$ *or* $v_R \leq Q'(0, w_L)$*, in which case* $v_M = v_R$ *and (b): the maximum possible velocity of upstream vehicles is lower than the downstream velocity, i.e.,* $v_R > V(0, w_L)$ *or* $v_R > Q'(0, w_L)$*. In this case, let* $v_M = V(0, w_L)$ *in order to minimize the gap to the downstream velocity.*

diate density ρ_{M}, s.t., $v_{\mathrm{M}} = V(\rho_{\mathrm{M}}, w_{\mathrm{L}})$.

These principles can be translated into the solver introduced in (11) and (12). One sees that the solver for the intermediate state in the 2CTM is consistent with that of the Riemann solver of the GOSM.

From the intuition to construct an intermediate traffic state, it is clear that the receiving potential of the downstream cell is determined by both the space that the downstream vehicles have created and the property of the upstream drivers. Considering an example that the upstream drivers are quite passive, and in contrast, the downstream cell is filled with aggressive drivers, then the receiving of vehicles depends not only on the amount of the space that the downstream vehicles can generate (determined by u_{R}), but also on the willingness of the vehicles from the upstream cell to fill the free space (determined by w_{L}). Therefore, it is not surprising that the receiving function (10) is also a function of the property of the upstream vehicles, which is different from the classical CTM.

2.2.5 A Multiple Model Framework for 2CTM

Next, a multiple model framework is proposed for the 2CTM by introducing the regime variable μ to describe the number of open lanes. Thus, the flow through a cell interface is a function of the regime variables of both the upstream and downstream cells. Following the same updating equations as the 2CTM (9), the inflow and outflow are defined as:

$$F^{\rho}_{j-1/2} = \min\left\{S\left(\rho^k_{j-1}, w^k_{j-1}, \mu^{k+1}_{j-1}\right),\ R\left(\rho^k_{j-1/2}, w^k_{j-1}, \mu^{k+1}_{j}\right)\right\},$$
$$F^{\rho}_{j+1/2} = \min\left\{S\left(\rho^k_{j}, w^k_{j}, \mu^{k+1}_{j}\right),\ R\left(\rho^k_{j+1/2}, w^k_{j}, \mu^{k+1}_{j+1}\right)\right\},$$

where μ^{k+1}_{j-1} and μ^{k+1}_{j} are the regime variables of the cells $j-1$ and j at time $t=(k+1)\Delta t$, and the sending and receiving functions (10) are modified to include the regime variable. Here $\rho^k_{j-1/2}$ and $\rho^k_{j+1/2}$ are the intermediate states (see Section 2.2.4). Generally, for two adjacent cells with traffic states u_{L} and u_{R}, the sending and receiving functions are:

$$\begin{aligned} S\left(\rho_{\mathrm{L}}, w_{\mathrm{L}}, \mu_{\mathrm{L}}\right) &= \begin{cases} \rho_{\mathrm{L}} v_{\mathrm{L}}, & \text{if } \rho_{\mathrm{L}} \le \mu_{\mathrm{L}}\rho_{\mathrm{c}}(w_{\mathrm{L}}), \\ Q^{w_{\mathrm{L}}}_{\max}(\mu_{\mathrm{L}}), & \text{if } \rho_{\mathrm{L}} > \mu_{\mathrm{L}}\rho_{\mathrm{c}}(w_{\mathrm{L}}), \end{cases} \\ R(\rho_{\mathrm{M}}, w_{\mathrm{L}}, \mu_{\mathrm{R}}) &= \begin{cases} Q^{w_{\mathrm{L}}}_{\max}(\mu_{\mathrm{R}}), & \text{if } \rho_{\mathrm{M}} \le \mu_{\mathrm{R}}\rho_{\mathrm{c}}(w_{\mathrm{L}}), \\ \rho_{\mathrm{M}}(\mu_{\mathrm{R}}) v_{\mathrm{M}}(\mu_{\mathrm{R}}), & \text{if } \rho_{\mathrm{M}} > \mu_{\mathrm{R}}\rho_{\mathrm{c}}(w_{\mathrm{L}}), \end{cases} \end{aligned} \tag{14}$$

where $v_{\mathrm{L}} = V\left(\rho_{\mathrm{L}}, w_{\mathrm{L}}, \mu_{\mathrm{L}}\right)$ is the upstream traffic velocity, $\rho_{\mathrm{M}}(\cdot)$ and $v_{\mathrm{M}}(\cdot)$ are the density and velocity of the intermediate state, and $Q^{w_{\mathrm{L}}}_{\max}(\mu_{\mathrm{L}})$ and $Q^{w_{\mathrm{L}}}_{\max}(\mu_{\mathrm{R}})$ are the maximum fluxes corresponding to the following flux function:

$$Q(\rho, w, \mu) = \rho V\left(\rho, w, \mu\right).$$

For example, one can define a velocity function as:

$$v = V(\rho, w, \mu) = \begin{cases} v_{\max}\left(1 - \frac{\rho}{\mu\tilde{\rho}_{\max}}\right), & \text{if} \quad \rho \le \mu\rho_{\mathrm{c}}(w), \\ \frac{Q^{w}_{\max}}{\mu(\rho_{\mathrm{c}}(w) - \rho_{\max}(w))}\frac{\rho - \mu\rho_{\max}(w)}{\rho}, & \text{if} \quad \rho > \mu\rho_{\mathrm{c}}(w), \end{cases} \tag{15}$$

where $\rho_{\max}(w) = \frac{\rho_{\max 1}\rho_{\max 2}}{w\rho_{\max 1}+(1-w)\rho_{\max 2}}$ and $\rho_{c}(w) = \frac{\rho_{c1}\rho_{c2}}{w\rho_{c1}+(1-w)\rho_{c2}}$. Here, the model parameters $\rho_{\max 1}$, $\rho_{\max 2}$, ρ_{c1} and ρ_{c2} are the upper and lower bounds of the jam density $\rho_{\max}$ and the critical density ρ_c, respectively, and $\tilde{\rho}_{\max}$ defines the curvature of the FD in the freeflow regime. All these parameters are defined with respect to a single lane, i.e., $\mu = 1$, and $Q^w_{\max} = \mu\rho_c(w)v_{\max}\left(1 - \frac{\rho_c(w)}{\tilde{\rho}_{\max}}\right)$.

Moreover, $\mu_L\rho_c(w_L)$ and $\mu_R\rho_c(w_L)$ are the corresponding critical densities such that these maximum fluxes are obtained. Note that $\rho_c(w_L)$ is the critical density with respect to the flux function of a single lane, i.e., $\mu = 1$. The maximum flows are calculated as:

$$Q^{w_L}_{\max}(\mu_L) = \mu_L\rho_c(w_L)V\left(\mu_L\rho_c, w_L, \mu_L\right), \qquad Q^{w_L}_{\max}\left(\mu_R\right) = \mu_R\rho_c(w_L)V\left(\mu_R\rho_c, w_L, \mu_R\right).$$

Next, the intermediate traffic density and velocity ρ_M and v_M are computed via a modified version of (12):

$$\begin{cases} w_M = w_L, \\ v_M = V(0, w_L, \mu_R), \quad \text{if} \quad V(0, w_L, \mu_R) < v_R, \\ v_M = v_R, \quad \text{otherwise}, \\ \rho_M, \quad \text{s.t.} \quad v_M = V(\rho_M, w_M, \mu_R), \end{cases} \tag{16}$$

where $v_R = V(\rho_R, w_R, \mu_R)$ is the velocity of the downstream vehicles.

Remark 2. In the definition of sending and receiving functions (14), the property is always chosen as the upstream property w_L. The sending function chooses the upstream regime variable μ_L, and the receiving function selects the downstream regime variable μ_R.

2.3 A Multiple Model 2CTM on Road Network

In Section 2.2, a multiple model framework for the 2CTM based on the GOSM is presented for a single road segment. It is desirable to generalize the model predictor to a road network since all traffic problems are solved with respect a network that is composed of links and junctions. In this case, a generalized Riemann problem is defined at each road junction. The methodology to construct a unique admissible solution to the junction Riemann problem by applying the GOSM or 2CTM is introduced next.

The key to compute the network solution requires defining a solution to a generalized Riemann problem at a junction located at x_0. Let the spatial domain of each incoming link i be given as $x_i \in \left(-\infty, x_{0,i}^-\right)$ and each outgoing link as $x_i \in \left(x_{0,i}^+, +\infty\right)$. Here, the point $x_{0,i}^-$ is the point on incoming link i which is immediately to the left of the junction at $x_{0,i}$, and $x_{0,i}^+$ is the point on outgoing link i immediately to the right of the junction. The junction Riemann problem is given as:

$$\begin{pmatrix} \rho_i \\ \rho_i w_i \end{pmatrix}_t + \begin{pmatrix} \rho_i v_i \\ \rho_i w_i v_i \end{pmatrix}_x = 0, \qquad u_i(x,0) = \begin{cases} u_i^- & \text{if} \quad x < x_{0,i}^-, \\ u_i^+ & \text{if} \quad x > x_{0,i}^+, \end{cases} \tag{17}$$

where ρ_i, w_i and v_i denote the density, property and velocity of vehicles on the ith link, respectively, and $u_i(x,t) = (\rho_i(x,t), \mu_i(x,t), \rho_i(x,t)w_i(x,t))$ is the traffic state, which is a function of both position x and time t. Note that the regime variables μ_i are involved. Moreover, $u_i^- = (\rho_i^-, \mu_i^-, \rho_i^- w_i^-)$ and $u_i^+ = (\rho_i^+, \mu_i^+, \rho_i^+ w_i^+)$ represent the constant initial data of the Riemann problem, and μ_i^- and μ_i^+ are the regime variables on an incoming link and an outgoing link.

The *Rankine–Hugoniot* conditions [24] are satisfied for piecewise constant solutions:

$$\sum_{i\in\delta^-} (\rho_i v_i)\left(x_{0,i}^-, t\right) = \sum_{i\in\delta^+} (\rho_i v_i)\left(x_{0,i}^+, t\right), \qquad \sum_{i\in\delta^-} (\rho_i v_i w_i)\left(x_{0,i}^-, t\right) = \sum_{i\in\delta^+} (\rho_i v_i w_i)\left(x_{0,i}^+, t\right), \tag{18}$$

where δ^- and δ^+ are the sets of incoming links and outgoing links, respectively. These two equations correspond to the conservation of mass ρ and conservation of the total property $y = \rho w$, respectively.

As pointed out in [20], condition (18) only is not sufficient to obtain a unique solution for the Riemann problem of a junction when applying a second order traffic model. Hence, additional conditions are necessary, such as: (i) a distribution parameter is specified that determines the priority rules of vehicles at a road junction, i.e.,

$$0 \leq a_{i,j} \leq 1, \quad \sum_{j \in \delta^+} a_{i,j} = 1, \quad \forall i \in \delta^-, \tag{19}$$

where $a_{i,j}$ is the percentage of vehicles from the ith incoming link that goes to the jth outgoing link; (ii) the total flux is maximized; (iii) the travel time is minimized. There are several other restrictions that are motivated by mathematical convenience in order to generate a unique solution at a junction. In this study, the distribution rule and traffic flow maximization rules are used.

In the framework of the GOSM, the quantity w represents a property of vehicles, and thus an admissible solution to a junction problem should guarantee that the upstream vehicles (vehicles from incoming links) preserve their property passing through a junction [24]. For example, drivers keep their property when driving from link i to link j. Recall the Remark 1 that the GOSM collapses to the LWR model by assuming a constant property. Similarly, it is shown later that forcing vehicles to retain their property when traveling through the junction is essential when solving a junction problem using the GOSM. When this is true, the junction problems are structurally similar to junction problems for the first order LWR model [10, 11] (excluding the merge problem).

Next, three types of junctions that are most common on a road network are studied: bottlenecks (e.g., lane drop), diverges (e.g., off–ramp), and merges (e.g., on–ramp).

2.3.1 Bottleneck: One Incoming Link and One Outgoing Link

A bottleneck is a simple network that involves two links $i = 1$ (incoming) and $i = 2$ (outgoing). Figure 6 shows a sample bottleneck junction where number of lanes changes from four lanes to three. The constant initial data for (17) is

$$u_1^- = (\rho_1^-, \mu_1^-, \rho_1^- w_1^-), \qquad u_2^+ = (\rho_2^+, \mu_2^+, \rho_2^+ w_2^+),$$

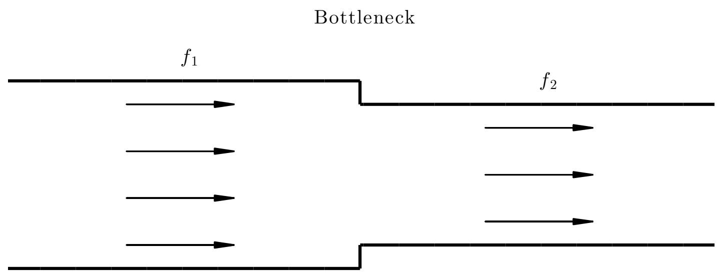

Figure 6: *Bottleneck junction.*

where $u_1(\cdot)$ and $u_2(\cdot)$ are traffic states on link 1 and link 2.

Vehicles with different properties interact with each other, and an intermediate state u_M is generated at the downstream side of the junction, i.e., at $x_{0,2}^+$ (see Section 2.2.4 for details). One sees that the intermediate state has the same property as the upstream vehicles since vehicles preserve their property, i.e., $u_\mathrm{M} = (\rho_\mathrm{M}, \rho_\mathrm{M} w_1^-)$. Next, the junction problem is solved between the states u_1^- and u_M, which have the same property w_1^-. This is equivalent to a junction problem for the LWR model.

The methodology to obtain a unique admissible solution to the junction problem applying the LWR model is introduced in [10, 11]. In summary, one solves a maximization problem

$$\begin{aligned} &\max f \\ &\text{s.t.} \quad 0 \leq f \leq S_1\left(\rho_1^-, w_1^-, \mu_1^-\right), \\ &\qquad\;\; 0 \leq f \leq R_2\left(\rho_\mathrm{M}, w_1^-, \mu_2^+\right), \end{aligned}$$

where f represents the realized flow across the junction, $S_1(\cdot)$ is the sending function of link 1, and $R_2(\cdot)$ represents the potential to receive vehicles on the link 2, which are defined in (14). Here, the receiving function is a function of the intermediate density ρ_M obtained from (16). Accordingly, the realized flow f^* between the links is the minimum of the sending and receiving functions:

$$f^* = \min\left\{S_1\left(\rho_1^-, w_1^-, \mu_1^-\right),\ R_2\left(\rho_\mathrm{M}, w_1^-, \mu_2^+\right)\right\}.$$

Based on the solver to the junction problem introduced in [10, 11], one obtains $u_1^* = (\rho_1^*, \rho_1^* w_1^*)$ and $u_2^* = (\rho_2^*, \rho_2^* w_2^*)$. Note that $w_1^* = w_2^* = w_1^-$. Then, an inverse problem is solved to obtain the densities given flows. The rules to obtain a unique solution are introduced in [10, 11].

For strictly concave flux functions, each flow value may correspond to two distinct densities, for a fixed property w and regime variable μ. On road i, one solves for density ρ_i^* given flow f_i^* as follows:

$$Q(\rho_i^*, w_i, \mu_i) = f_i^*, \qquad Q(\rho_i^*, w_i, \mu_i) = \rho_i^* V_i(\rho_i^*, w_i, \mu_i),$$

where w_i and μ_i are the property quantity and the regime variable on road i, and $V_i(\cdot)$ is the velocity function of the road i. For a given flow f_i^*, two distinct density solutions may generated. The unique density solution is selected from the following rules. For the ith incoming link, the density solution belongs to domain $\mathcal{D}_{\text{in}}^i$ that is defined as

$$\rho_i^* \in \mathcal{D}_{\text{in}}^i = \begin{cases} \{\rho_i^-\} \cup \left(\Lambda(\rho_i^-),\ \mu_i^- \rho_{\max}(w_i^-)\right], & \text{if} \quad 0 \le \rho_i^- \le \mu_i^- \rho_{\text{c}}(w_i^-), \\ \left[\mu_i^- \rho_{\text{c}}(w_i^-),\ \mu_i^- \rho_{\max}(w_i^-)\right], & \text{if} \quad \mu_i^- \rho_{\text{c}}(w_i^-) \le \rho_i^- \le \mu_i^- \rho_{\max}(w_i^-), \end{cases} \tag{20}$$

where ρ_i^-, w_i^- and μ_i^- represent the density, property and regime variable of the ith incoming road, respectively, and $\rho_{\text{c}}(\cdot)$ and $\rho_{\max}(\cdot)$ are the critical density and the maximum density that depend on w. Here, they are defined with respect to a single lane, i.e., $\mu = 1$. Moreover, $\Lambda(\cdot)$ is defined such that $Q\left(\rho, w, \mu\right) = Q\left(\Lambda(\rho), w, \mu\right)$, for $\rho \in [0, \mu\rho_{\max}(w)]$. For example, $\Lambda(0) = \mu_i \rho_{\max}(w_i)$ on road i. Similarly, the unique density solution on the jth outgoing road ρ_j^* belongs to the domain $\mathcal{D}_{\text{out}}^j$ that is defined as

$$\rho_j^* \in \mathcal{D}_{out}^j = \begin{cases} \left[0,\ \mu_j^+ \rho_{\text{c}}(w_j^+)\right], & \text{if} \quad 0 \le \rho_j^+ \le \mu_j^+ \rho_{\text{c}}(w_j^+), \\ \left\{\rho_j^+\right\} \cup \left[0,\ \Lambda(\rho_j^+)\right), & \text{if} \quad \mu_j^+ \rho_{\text{c}}(w_j^+) \le \rho_j^+ \le \mu_j^+ \rho_{\max}(w_j^+), \end{cases} \tag{21}$$

where where ρ_j^+, w_j^+ and μ_j^+ are the density, property and regime variable of the jth outgoing

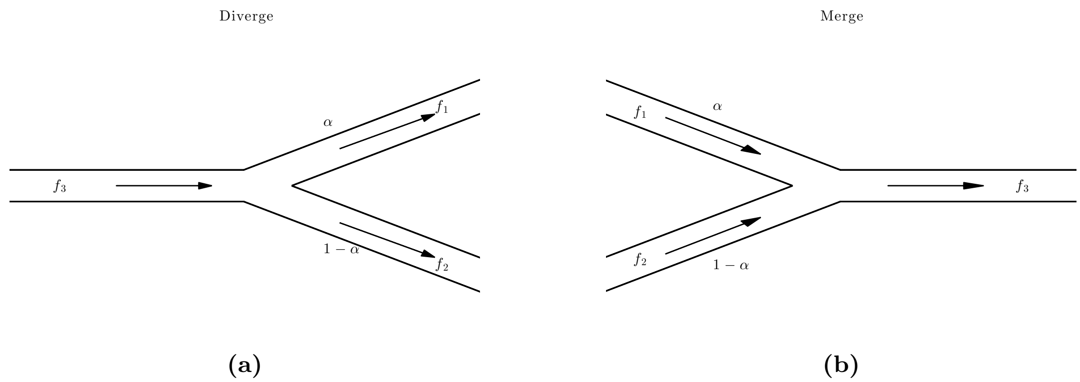

Figure 7: *(a) is a diverge junction, and (b) is a merge junction.*

road. In summary, the inverse problem that gives a unique solution is

$$\begin{aligned} Q\left(\rho_i^*, w_i^-, \mu_i^-\right) &= f_i^*, \quad \rho_i^* \in \mathcal{D}_{\text{in}}^i, \quad\ \ i \in \delta^-, \\ Q\left(\rho_j^*, w_j^+, \mu_j^+\right) &= f_j^*, \quad \rho_j^* \in \mathcal{D}_{\text{out}}^j, \quad j \in \delta^+, \end{aligned} \tag{22}$$

where δ^- and δ^+ are the sets of incoming links and outgoing links, respectively, and $\mathcal{D}_{\text{in}}^i$ and $\mathcal{D}_{\text{out}}^j$ are defined in (20) and (21).

Next, two initial boundary value problems are solved on each road segment to obtain weak entropy solutions $u_1(x,t)$ and $u_2(x,t)$:

$$\begin{aligned} (u_i)_t + (v_i u_i)_x = 0, \qquad i = 1,\ 2, \\ u_1(x,0) = \begin{pmatrix} u_1^-, & \text{if} \quad x < x_{0,1}^- \\ u_1^*, & \text{if} \quad x \geq x_{0,1}^- \end{pmatrix}, \\ u_2(x,0) = \begin{pmatrix} u_2^*, & \text{if} \quad x \leq x_{0,2}^+ \\ u_2^+, & \text{if} \quad x > x_{0,2}^+ \end{pmatrix}. \end{aligned} \tag{23}$$

2.3.2 Diverge: One Incoming Link and Two Outgoing Links

The initial value problem (17) of a diverge junction (see Figure 7a) uses the following constant initial data:

$$\begin{cases} u_1^+ = (\rho_1^+, \mu_1^+, \rho_1^+ w_1^+), \\ u_2^+ = (\rho_2^+, \mu_2^+, \rho_2^+ w_2^+), \end{cases} \qquad u_3^- = (\rho_3^-, \mu_3^-, \rho_3^- w_3^-).$$

where $i = 1,\ 2$ represent the two outgoing links, and $i = 3$ denotes the incoming link. Similar to the bottleneck problem, the Riemann problem of a diverge junction can also be reduced to the classical network problem for the LWR model.

The solver proceeds in two steps:

1. Two intermediate states $u_i^{\mathrm{M}} = \left(\rho_i^{\mathrm{M}}, \rho_i^{\mathrm{M}} w_i^{\mathrm{M}}\right)$, $i = 1, 2$ are generated at the starting points of two outgoing links, i.e., at the positions a_1 and a_2, with $w_1^{\mathrm{M}} = w_2^{\mathrm{M}} = w_3^-$. Again, these intermediate states exist because drivers with different properties (from the upstream or incoming links) try to match the velocity of the downstream vehicles (the outgoing links) at a junction.

2. A junction problem is solved with initial data u_1^{M}, u_2^{M} and u_3^-. One sees that this is a network problem based on the LWR model (see [10, 11] for detail) since the property quantities are the same. The solutions are represented as u_1^*, u_2^*, and u_3^*. In particular, $w_1^* = w_2^* = w_3^* = w_3^-$.

One refers to (16) to solve for the intermediate states in the first step. For the second step, the allocation rule (19) is imposed to render a unique solution, as presented in [10, 11, 24].

For a diverge problem, the following maximization problem is solved (see Figure 8):

$$\begin{aligned} &\max\,(f_1 + f_2) \\ &\qquad \text{s.t.} \quad 0 \leq f_i \leq R_i\left(\rho_i^{\mathrm{M}}, w_3^-, \mu_i^+\right), \quad i = 1,\ 2, \\ &\qquad\qquad\;\; 0 \leq f_1 + f_2 \leq S_3\left(\rho_3^-, w_3^-, \mu_3^-\right), \end{aligned} \tag{24}$$

where $R_i(\cdot)$, $i = 1, 2$ are the receiving functions on the outgoing links (downstream), and

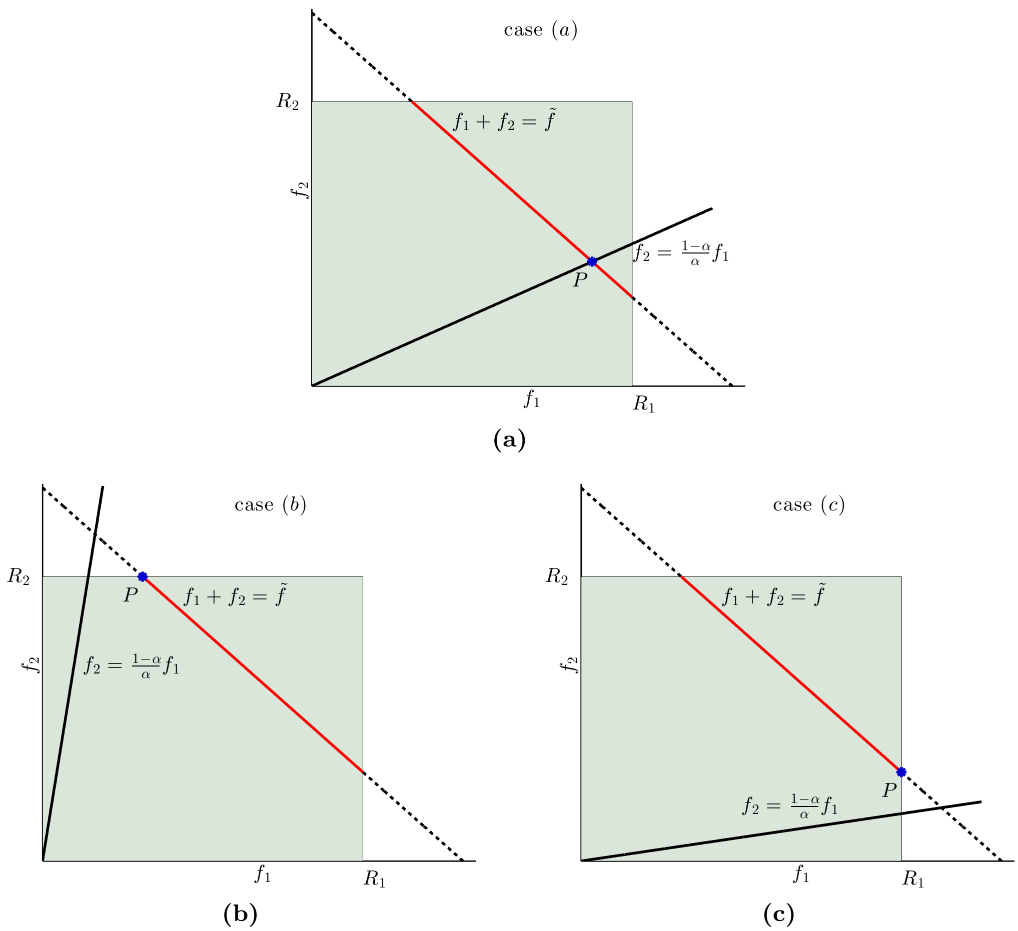

Figure 8: *Maximization problem for diverge junction. Here, three cases (a), (b), (c) illustrate different selections of priority rule. The points P that are marked blue–star represent the solutions which maximize the inflow or outflow.*

$S_3(\cdot)$ is the sending function from the incoming link (upstream) (16). Again, the receiving functions are functions of the intermediate traffic densities ρ_i^{M}, $i = 1, 2$, and they depend on the upstream property w_3^-. This maximization problem is equivalent to

$$\tilde{f} = \max\{f_1 + f_2\} = \min\left\{R_1\left(\rho_1^{\mathrm{M}}, w_3^-, \mu_1^+\right) + R_2\left(\rho_2^{\mathrm{M}}, w_3^-, \mu_2^+\right),\ S_3\left(\rho_3^-, w_3^-, \mu_3^-\right)\right\}. \quad (25)$$

Without the priority rules specified by (19), infinitely many solutions are generated that satisfy:

$$f_1 + f_2 = \tilde{f}, \qquad (f_1, f_2) \in \Omega, \quad (26)$$

where $\Omega = [0,\ R_1\left(\rho_1^{\mathrm{M}}, w_3^-, \mu_1^+\right)] \times [0, R_2\left(\rho_2^{\mathrm{M}}, w_3^-, \mu_2^+\right)] \subset \mathbb{R}^2$ (see the interval that is marked with red color in Figure 8). Note that on this interval (26), flow is maximized. In particular, the interval (26) shrinks to a single point if $\tilde{f} = R_1 + R_2$, which is respect to the case when $R_1 + R_2 < S_3$.

Here, a distribution rule (19) is specified, where $a_{3,1}$ is the percentage of vehicles from link 3 that goes to link 1, and $a_{3,2}$ represents the portion that goes to link 2. For notational convenience, letting $\alpha = a_{3,1}$, and $(1 - \alpha) = a_{3,2}$, a unique solution is obtained for each of the three cases (see Figure 8) based on different priority rules. The priority rule is as follows:

$$\frac{f_2}{f_1} = \frac{(1-\alpha)\tilde{f}}{\alpha\tilde{f}} = \frac{1-\alpha}{\alpha} = \kappa. \quad (27)$$

Whenever possible, vehicles traveling through a diverge junction should follow the priority rule (27). Note that the interval (26) at the point does not necessarily intersect with the linear function defined by the priority rule. In these cases, the solution is selected on the interval (26) that has the smallest distance to the line (27) (see Figs. 8b, 8c).

In case (a) (see Fig. 8a), the solution is the unique intersection

$$f_1^* = \frac{\tilde{f}}{1+\kappa}, \qquad f_2^* = \frac{\kappa\tilde{f}}{1+\kappa}.$$

In case (b) (see Fig. 8b), the solution is

$$f_1^* = \tilde{f} - R_2, \qquad f_2^* = R_2.$$

In case (c) (see Fig. 8c), the solution is

$$f_1^* = R_1, \qquad f_2^* = \tilde{f} - R_1.$$

In case (a) and case (b), the solution no longer follows the priority rule in order to maximize the traffic flow. Instead, flow is maximized and the priority rule is obeyed [10]. Then, inverse problem (22) is solved to obtain the densities ρ_i^* given the flows f_i^*.

Next, by applying the solutions of the junction problem to the Riemann problem defined in (17), three initial value problems are solved on each road segment:

$$\begin{aligned} &(u_i)_t + (v_i u_i)_x = 0, \qquad i = 1,\ 2,\ 3, \\ &u_i(x,0) = \begin{pmatrix} u_i^*, & \text{if} \quad x \le x_{0,i}^+ \\ u_i^+, & \text{if} \quad x > x_{0,i}^+ \end{pmatrix}, \qquad i = 1,\ 2, \\ &u_3(x,0) = \begin{pmatrix} u_3^-, & \text{if} \quad x < x_{0,3}^- \\ u_3^*, & \text{if} \quad x > x_{0,3}^- \end{pmatrix}. \end{aligned} \tag{28}$$

2.3.3 Merge: Two Incoming Links and One Outgoing Link

The initial value problem (17) for a merge junction (see Figure 7b) is defined using the following constant initial data.

$$\begin{cases} u_1^- = \left(\rho_1^-, \mu_1^-, \rho_1^- w_1^-\right), \\ u_2^- = (\rho_2^-, \mu_2^-, \rho_2^- w_2^-), \end{cases} \qquad u_3^+ = \left(\rho_3^+, \mu_3^+, \rho_3^+ w_3^+\right),$$

where $i = 1,\ 2$ denote the incoming links, and $i = 3$ is the outgoing link. Mathematically, merge problem is equivalent to the diverge problem for the LWR model [10, 11]. For the

GOSM, there is an important distinction between these two types of junctions: *the property on the outgoing link is defined in an average sense, which depends on the flows from the two incoming links, i.e.,*:

$$w_3^* = \frac{w_1^- f_1 + w_2^- f_2}{f_1 + f_2}, \tag{29}$$

where w_3^* represents the property on the outgoing link, and f_1 and f_2 are the flows from two incoming links.

To see this distinction more clearly, one investigates the following maximization problem:

$$\begin{aligned} &\max\left(f_1 + f_2\right) \\ &\quad \text{s.t.} \quad 0 \leq f_i \leq S_i\left(\rho_i^-, w_i^-, \mu_i^-\right), \quad i = 1,\ 2, \\ &\qquad\qquad 0 \leq f_1 + f_2 \leq R_3\left(\rho_3^{\mathrm{M}}, w_3^*, \mu_3^+\right), \quad \text{with} \quad \rho_3^{\mathrm{M}} = \rho_3^{\mathrm{M}}(u_3^+, w_3^*), \end{aligned} \tag{30}$$

where the intermediate state $\rho_3^{\mathrm{M}}(\cdot)$ is computed from (16), which depends on both the downstream state u_3^+ and the property of vehicles from the upstream w_3^{M}. Note that the maximization problem (30) is a nonlinear optimization problem, since the receiving function depends on w^*, which itself depends on f_1 and f_2. In this work, a different method is applied to obtain a unique solution for the merge junction [24].

Based on the discussion in [24], the nonlinear optimization problem can be simplified to a linear optimization problem by forcing the vehicles to follow the priority rule (19). Here, the priority rule is recognized as a *mixture rule* that describes how vehicles of incoming links mix when they enter the outgoing link. Let α be the percentage of vehicles from the first incoming link, with $\alpha > 0$, and $(1 - \alpha)$ be the portion of vehicles from the second incoming link. The property on the outgoing link is given as

$$w_3^* = \alpha w_1^- + (1 - \alpha) w_2^-, \tag{31}$$

which is independent of the flows from two incoming links f_1 and f_2. Note that the mixture rule in a merge problem must be satisfied, and therefore the flow is not necessarily maximized.

Fixing the priority rule, the following linear optimization problem is solved:

$$
\begin{aligned}
&\max\left(f_1+f_2\right)\\
&\quad \text{s.t.}\quad f_2=\kappa f_1,\\
&\qquad\quad 0\le f_i\le S_i\left(\rho_i^-,w_i^-,\mu_i^-\right),\quad i=1,\ 2\\
&\qquad\quad 0\le f_1+f_2\le R_3\left(\rho_3^{\mathrm{M}},w_3^*,\mu_3^+\right),
\end{aligned}
\tag{32}
$$

where κ is defined as (27), and ρ_3^{M} is the intermediate state, where the property w_3^* is calculated by (31). The unique solution is therefore

$$
f_1^*=\min\left\{S_1,S_2/\kappa,R_3/(1+\kappa)\right\},\quad f_2^*=\kappa f_1^*,\quad f_3^*=(1+\kappa)f_1^*. \tag{33}
$$

Next, the density solutions ρ_i^* are obtained by solving the inverse problem (22). Moreover, $w_1^*=w_1^-$, $w_2^*=w_2^-$, and w_3^* is determined by (31)

Similar to the diverge problem, the following initial value problems are solved:

$$
\begin{aligned}
&\left(u_i\right)_t+\left(v_iu_i\right)_x=0,\qquad i=1,\ 2,\ 3,\\
&\qquad u_i(x,0)=\begin{pmatrix} u_i^-, & \text{if} & x<x_{0,i}^-\\ u_i^*, & \text{if} & x\ge x_{0,i}^-\end{pmatrix},\qquad i=1,\ 2,\\
&\qquad u_3(x,0)=\begin{pmatrix} u_3^*, & \text{if} & x\le x_{0,3}^+\\ u_3^+, & \text{if} & x> x_{0,3}^+\end{pmatrix},
\end{aligned}
\tag{34}
$$

where u_1^*, u_2^*, and u_3^* are the solutions to the merge junction problem. Next, an approximate solver to network problems is developed based on the multiple model 2CTM. As shown in the next section, only the f^* and w^* are necessary in the discrete formulation.

Remark 3. The solution does not necessarily maximize the flow. For instance, consider the case there are no vehicles on the first incoming link. The physically meaningful solution that maximizes the traffic flow has $f_1^*=0$. By (29), one obtains $w_3^*=w_2^-$, which contradicts (31).

2.3.4 A Multiple Model Framework on a Road Network

In this section, the multiple model 2CTM on a road network is summarized.

Generally, one considers an incoming link i, where the cell adjacent to the junction is the nth cell. The update equations for the nth cell on each link i is given by:

$$\begin{aligned} \rho_{i,n}^{k+1} &= \rho_{i,n}^{k} + \frac{\Delta t}{\Delta x}\left(F_{i,n-1/2}^{\rho} - f_i^*\right), \\ y_{i,n}^{k+1} &= y_{i,n}^{k} + \frac{\Delta t}{\Delta x}\left(w_{i,n-1}^{k} F_{i,n-1/2}^{\rho} - w_i^* f_i^*\right). \end{aligned} \tag{35}$$

where $\rho_{i,n}^k$ and $\rho_{i,n}^{k+1}$ are traffic densities of the cell i, at time $t = k\Delta t$ and $t = (k+1)\Delta t$, respectively, and $y_{i,n}^k$ and $y_{i,n}^{k+1}$ are the associated quantities of total properties, e.g., $y_{i,n}^k = w_{i,n}^k \rho_{i,n}^k$, where $w_{i,n}^k$ represents the property of vehicles in the cell. Moreover, $F_{i,n-1/2}^{\rho}$ is the inflow of the cell i, and the outflow f_i^* is the solution to the junction problem at the ith incoming link. Furthermore, $w_i^* = w_{i,n}^k$, i.e., the property always follows that of the upstream flow.

Similarly, for an outgoing link j, the evolution equations at the first cell of the jth outgoing link are

$$\begin{aligned} \rho_{j,1}^{k+1} &= \rho_{j,1}^{k} + \frac{\Delta t}{\Delta x}\left(f_j^* - F_{j,3/2}^{\rho}\right), \\ y_{j,1}^{k+1} &= y_{j,1}^{k} + \frac{\Delta t}{\Delta x}\left(w_j^* f_j^* - w_{j,1}^{k} F_{j,3/2}^{\rho}\right), \end{aligned} \tag{36}$$

where f_j^* and $F_{j,3/2}^{\rho}$ are the upstream and downstream flows of the cell. The inflow f_j^* and the upstream property w_j^* are the solutions of the junction problem. The solvers for a diverge network and a merge network are summarized in Algorithm 2 and Algorithm 3, respectively.

2.4 A Hybrid State Estimation Problem

The challenges for solving the proposed hybrid state estimation problem are due to the non-linearities and switching dynamics associated with the traffic model. In the past, a number of techniques in the estimation community have been developed to solve hybrid estimation

Algorithm 2 *Network Solver: Diverge*

Current Time Step ($t = k\Delta t$): initial traffic states in the initial cells of two outgoing links (cell one for link one and link two), and the end cell (nth cell) of the incoming link three: $u^k_{1,1} = \left(\rho^k_{1,1}, \mu^k_{1,1}, \rho^k_{1,1} w^k_{1,1}\right)$, $u^k_{2,1} = \left(\rho^k_{2,1}, \mu^k_{2,1}, \rho^k_{2,1} w^k_{2,1}\right)$, and $u^k_{3,n} = \left(\rho^k_{3,n}, \mu^k_{3,n}, \rho^k_{3,n} w^k_{3,n}\right)$.
Intermediate State: Two intermediate states $u^{\mathrm{M}}_{i,1} = (\rho^{\mathrm{M}}_{i,1}, \rho^{\mathrm{M}}_{i,1} w^{\mathrm{M}}_{i,1})$, $i = 1, 2$ are generated at the left bounds of the first cells.

- Because vehicles conserve their property through the junction, one obtains $w^{\mathrm{M}}_{1,1} = w^{\mathrm{M}}_{2,1} = w^k_{3,n}$.
- The intermediate densities $\rho^{\mathrm{M}}_{1,1}$ (between $u^k_{3,n}$ and $u^k_{1,1}$) and $\rho^{\mathrm{M}}_{2,1}$ (between $u^k_{3,n}$ and $u^k_{2,1}$) are computed from (16):

$$\rho^{\mathrm{M}}_{1,1} = \mathrm{argmin}_\rho \left\{ V\left(\rho^k_{1,1}, w^k_{1,1}, \mu^k_{1,1}\right) - V\left(\rho, w^k_{3,n}, \mu^k_{3,n}\right)\right\},$$
$$\rho^{\mathrm{M}}_{2,1} = \mathrm{argmin}_\rho \left\{ V\left(\rho^k_{2,1}, w^k_{2,1}, \mu^k_{2,1}\right) - V\left(\rho, w^k_{3,n}, \mu^k_{3,n}\right)\right\}.$$

Solve Junction Problem: A diverge junction problem is solved with initial data $u^{\mathrm{M}}_{1,1}$, $u^{\mathrm{M}}_{2,1}$ and $u^k_{3,n}$. Here, (25) is solved, and f^*_1, f^*_2, and f^*_3 are chosen to obey the priority rule (27) as much as possible. Moreover, $w^*_1 = w^*_2 = w^*_3 = w^k_{3,n}$.
Next Time Step ($t = (k+1)\Delta t$): the traffic density and the total property $y = \rho w$ are updated to the next time step:

- In cell one for link one and link two (outgoing links):

$$\begin{aligned}
\rho^{k+1}_{i,1} &= \rho^k_{i,1} + \frac{\Delta t}{\Delta x}\left(f^*_i - F^\rho_{i,3/2}\right), \\
y^{k+1}_{i,1} &= y^k_{i,1} + \frac{\Delta t}{\Delta x}\left(w^*_i f^*_i - w^k_{i,1} F^\rho_{i,3/2}\right), \qquad i = 1,\ 2, \\
w^{k+1}_{i,1} &= y^{k+1}_{i,1} / \rho^{k+1}_{i,1}.
\end{aligned}$$

- In cell n for link three (incoming link):

$$\begin{aligned}
\rho^{k+1}_{3,n} &= \rho^k_{3,n} + \frac{\Delta t}{\Delta x}\left(F^\rho_{3,n-1/2} - f^*_3\right), \\
y^{k+1}_{3,n} &= y^k_{3,n} + \frac{\Delta t}{\Delta x}\left(w^k_{3,n-1} F^\rho_{3,n-1/2} - w^*_3 f^*_3\right), \\
w^{k+1}_{3,n} &= y^{k+1}_{3,n} / \rho^{k+1}_{3,n}.
\end{aligned}$$

- In all other cells: apply the multiple model 2CTM (see Section 2.2.5).

Algorithm 3 *Network Solver: Merge*

Current Time Step ($t = k\Delta t$): initial traffic states in the end cells of link one and link two, and the initial cell of the incoming link three: $u^k_{1,n_1} = \left(\rho^k_{1,n_1}, \mu^k_{1,n_1}, \rho^k_{1,n_1} w^k_{1,n_1}\right)$, $u^k_{2,n_2} = \left(\rho^k_{2,n_2}, \mu^k_{2,n_2}, \rho^k_{2,n_2} w^k_{2,n_2}\right)$, and $u^k_{3,1} = \left(\rho^k_{3,1}, \mu^k_{3,1}, \rho^k_{3,1} w^k_{3,1}\right)$.

Intermediate State: An intermediate state $u^{\mathrm{M}}_{3,1} = (\rho^{\mathrm{M}}_{3,1}, \rho^{\mathrm{M}}_{3,1} w^{\mathrm{M}}_{3,1})$ is generated at the left bound of link three.

- By the mixture rule (19), one obtains $w^{\mathrm{M}}_{3,1} = \alpha w^k_{1,n_1} + (1-\alpha) w^k_{2,n_2}$.
- By (12), the intermediate density $\rho^{\mathrm{M}}_{3,1}$ is generated

$$\rho^{\mathrm{M}}_{3,1} = \mathrm{argmin}_\rho \left\{ V\left(\rho^k_{3,1}, w^k_{3,1}, \mu^k_{3,1}\right) - V\left(\rho, w^{\mathrm{M}}_{3,1}, \mu^k_{3,1}\right) \right\}.$$

Solve Junction Problem: A merge junction problem is solved with initial data u^k_{1,n_1}, u^k_{2,n_2} and $u^{\mathrm{M}}_{3,1}$. Here, (33) is solved for f^*_1, f^*_2, and f^*_3. Moreover, $w^*_1 = w^k_{1,n_1}$, $w^*_2 = w^k_{2,n_2}$, and $w^*_3 = w^{\mathrm{M}}_{3,1}$.

Next Time Step ($t = (k+1)\Delta t$): the traffic density and the total property $y = \rho w$ are updated to the next time step:

- In cells n for link one and link two (incoming links):

$$\begin{aligned} \rho^{k+1}_{i,n_i} &= \rho^k_{i,n_i} + \frac{\Delta t}{\Delta x}\left(F^\rho_{i,n_i-1/2} - f^*_i\right), \\ y^{k+1}_{i,n_i} &= y^k_{i,n_i} + \frac{\Delta t}{\Delta x}\left(w^k_{i,n_i-1} F^\rho_{i,n_i-1/2} - w^*_i f^*_i\right), \qquad i = 1,\ 2, \\ w^{k+1}_{i,n_i} &= y^{k+1}_{i,n_i} / \rho^{k+1}_{i,n_i}. \end{aligned}$$

- In cell one for link three (outgoing link):

$$\begin{aligned} \rho^{k+1}_{3,1} &= \rho^k_{3,1} + \frac{\Delta t}{\Delta x}\left(f^*_3 - F^\rho_{3,3/2}\right), \\ y^{k+1}_{3,1} &= y^k_{3,1} + \frac{\Delta t}{\Delta x}\left(w^*_3 f^*_3 - w^k_{3,1} F^\rho_{3,3/2}\right), \\ w^{k+1}_{3,1} &= y^{k+1}_{3,1} / \rho^{k+1}_{3,1}. \end{aligned}$$

- In all other cells: apply the multiple model 2CTM (see Section 2.2.5).

problems in the form of (1).

The *multiple model particle filter* (MMPF) [47] solves the hybrid state estimation problem by allowing the system to have several models. It has a model transition step that describes the switching dynamics of the system mode, and particles are generated for likely system models. The idea of the MMPF is that if the state u^k generated by a model variable μ^k matches well with the measurements, then the estimator believes the system is operating in model μ at time k. One central challenge for the MMPF to work in practice is due to its large computational load. When a system has multiple models and some models have very low probability of occurrence (e.g., system fault detection, traffic incident detection), the estimation algorithm requires a large sample size so as to generate enough samples for all possible models of the system. This will lead to a large computational load and possibly prevent the algorithms from being implemented in real time. This problem is addressed by [49], where a model–conditioned PF algorithm is proposed as an modification to the standard MMPF. The computation time can be significantly reduced using this algorithm when a hybrid state system contains rare modes.

Another group of the estimation techniques for solving the hybrid state estimation problem exploits the *multiple model* (MM) approach and the Kalman filter. One of the widely used approaches is the *interactive multiple model* (IMM) Kalman filter [7, 37, 43]. This method is a model–conditioned Kalman filtering approach. It first computes the weights for all the models of the hybrid system based on the switching probabilities among the models. Then, a Kalman filter is performed on each model. The choice of the Kalman filter (e.g., extended Kalman filter, EnKF, unscented Kalman filter) is problem dependent. The system state is estimated by the estimation results from each model–conditioned Kalman filter and the weight of each model computed by transitional probabilities among the system models.

Recently, the MMPF has been deployed for traffic state estimation and incident detection in [51]. A multiple model particle filter is used to accommodate the nonlinearity and the switching dynamics of the traffic incident model based on the scalar LWR traffic model. The solution is a posterior distribution of system state u and system model μ. In this work, we apply the MMPF to the second order traffic flow model (3). The multiple model particle filter algorithm proposed in [51] is summarized in Algorithm 4.

Algorithm 4 *Multiple model particle filter [47]*

Initialization ($k = 0$): generate M samples τ_l^0 and assign equal weights $\zeta_l^0 = 1/M$, where $l = 1, \cdots, M$
for $k = 1$ to $k_{\max}$ **do**
  Regime transition: $\mu_l^k = \Pi\left(\mu_l^{k-1}\right)$ for all l
  Prediction: $u_l^k = \mathcal{F}\left(u_l^{k-1}, \mu_l^k\right) + \eta^{k-1}$ for all l
  Measurement processing:
  calculate the likelihood: $p\left(z^k|\tau_l^k\right)$ for all l
  update weights: $\zeta_l^k = \zeta_l^{k-1} p\left(z^k|\tau_l^k\right)$ for all l
  normalize weights: $\hat{\zeta}_l^k = \zeta_l^k / \sum_{l=1}^{M} \zeta_l^k$ for all l
  Resampling: multiply/ suppress samples τ_l^k with high/ low importance weights $\hat{\zeta}_l^k$
  Output: posterior distribution of u^k and μ^k
  Reassign weights: $\zeta_l^k = 1/M$ for all l
  $k = k + 1$
end for

Since the objective of the algorithm is to jointly estimate the traffic state u^k and the model variable μ^k, the algorithm defines an augmented state as $\tau^k = (u^k, \mu^k)$, which is to be estimated.

The regime variable is modeled as a g state first-order Markov chain [47] with transition probabilities defined by:

$$\pi_{ed} = p\left\{\mu_k = d|\mu_{k-1} = e\right\}, \quad e, d \in \Gamma, \tag{37}$$

where the set Γ defines all possible incident conditions. The transition probability matrix is defined as $\Pi = [\pi_{ed}]$, which is a $g \times g$ matrix satisfying

$$\pi_{ed} \geq 0 \quad \text{and} \quad \sum_{e=1}^{g} \pi_{ed} = 1. \tag{38}$$

Equation (37) indicates the probability of the transition from one model to another. In the traffic incident detection problem, it specifies how many lanes will likely be open at each time step.

The MMPF works as follows. First, the algorithm constructs an initial distribution of the augmented system state τ^k based on the prior knowledge. Here, the notation l is used to index the particles. At the initial time step, all the particles are assigned with equal weights. Then, according to the transition probability and the model variable from the previous time step, for each particle, the algorithm determines the model variable for the current time step. Next, the model prediction step is performed to calculate the prior distribution of the system state u^k. This gives the prediction by the traffic model. When the measurement for the current time step is obtained, the algorithm computes the likelihood of each particle and updates the weight of each particle based on the computed likelihood and its previous weight. Finally, the algorithm resamples the particles based on their weights. During resampling, if a particle has a high weight, the algorithm will generate more of that particle, while particles with low weights are removed from the sample set.

The idea of the MMPF is that if a particle is generated by the correct model for the current time step, it should match well with the measurements received from the sensor. Consequently, the particle will be assigned with high weight and treated more importantly in the posterior distribution. Similarly, if a particle is generated by a wrong model, it will not match with well the measurements, and be assigned with less weight. Then, after resampling, the particle will be removed from the sample set.

2.5 Simulation Results Based on CORSIM

We test the MMPF (Algorithm 4) applied to a second order traffic flow model (3) through a numerical experiment using CORSIM, where the true state is known. CORSIM is a microscopic traffic simulation software developed by the Federal Highway Administration [42], which is constructed from car–following and lane switching models. This microscopic simulator is very different from the second order macroscopic traffic flow model used in the estimation algorithm, and therefore provides a more realistic simulation platform to test the

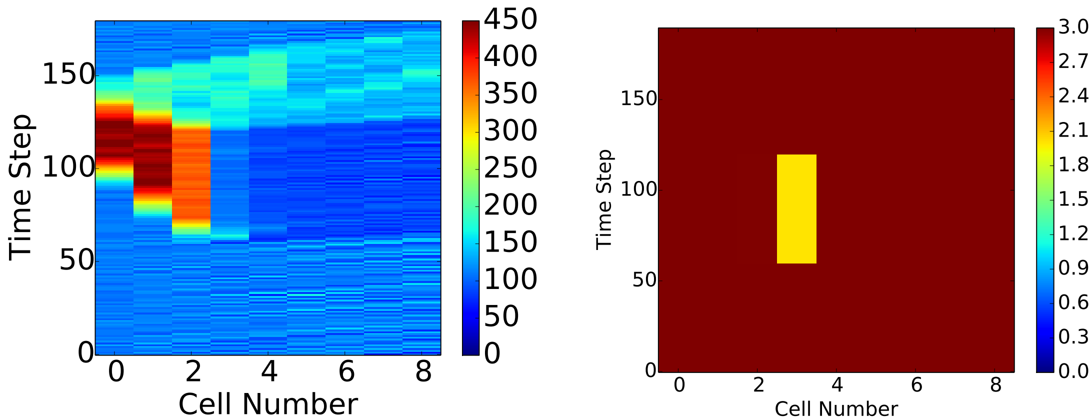

(a) Density (veh/mile) **(b)** Model variable (lanes open)

Figure 9: *True evolution of the traffic density and the model variable.*

algorithm.

To generate the true state to be estimated, a CORSIM simulation is performed on a 4 mile highway with a speed limit of 65 mph. The simulation time is one hour (180 30-second timesteps). An incident is created in cell four, which is 1.36 miles from the starting point of the highway. The incident starts 20 minutes after the simulation starts and lasts for 20 minutes (i.e. from time step 60 to time step 120 in the traffic model). The evolutions of the traffic density and model parameter are shown in Figs. 9a and 9b.

Next, synthetic GPS measurements are created by extracting the trajectory data from the CORSIM simulation. Various subsets of the vehicles are selected as probe vehicles, and speed measurements are generated from these vehicles to simulate GPS measurements. In this work, the penetration rate of GPS equipped vehicles is specified by adjusting the headway between these vehicles.

In order to run the second order traffic flow model, the fundamental diagram shape and parameters must be determined. Because the velocity function must be strictly decreasing with respect to the density in the second order model, a piecewise quadratic fundamental diagram is selected:

$$Q(\rho, w, \mu) = \begin{cases} v_{\max}\rho\left(1 - \rho/\mu\bar{\rho}\right) & \text{if } \rho \leq \mu\rho_c \\ a(w,\mu)\rho^2 + b(w,\mu)\rho + c(w,\mu) & \text{if } \rho \geq \mu\rho_c, \end{cases} \tag{39}$$

To calibrate the parameters of the fundamental diagram, a number of CORSIM simulations were generated under a range of different traffic conditions. In each simulation, the densities and speeds were recorded to simulate data available from an inductive loop detector. To fit this data, the parameters of the fundamental diagram were set as $v_{\max} = 65$ mph, $\rho_{\max}$ ranges from 235-245 vpm/lane, $Q_{\max}$ ranges from 2100 - 2700 vph/lane, and $\bar{\rho}$ is 30000 vpm/lane. The large value of $\bar{\rho}$ forces the quadratic function in free flow to closely approximate a linear function. Finally, the parameters a, b, and c in (39) are a function of w and can be determined by solving the following system of equations:

$$\begin{cases} a\mu\rho_{max}(w)^2 + b\mu\rho_{max}(w) + c = 0 \\ -\frac{b}{2a} = \frac{\mu Q_{\max}^w}{v_{\max}} \\ \frac{4ac-b^2}{4a} = \mu Q_{\max}^w, \end{cases} \tag{40}$$

where $\rho_{\max}(w) = w\rho_{\max1} + (1-w)\rho_{\max2}$ and $Q_{\max}^w = wq_{\max1} + (1-w)q_{\max2}$ Here, $\rho_{\max1}$ and $\rho_{\max2}$ are the upper and lower bounds of the maximum traffic density, $q_{\max1}$ and $q_{\max2}$ are the upper of lower bounds of the maximum flow in the second order traffic model. The resulting fundamental diagram for the second order traffic model is shown in Figure 10 for several values of w.

Several numerical experiments are run by implementing the MMPF on the second order traffic model, and generating measurements uisng different headways between GPS vehicles. In the numerical simulation, we run the proposed algorithm with 1000 particles. We assume there is no incident with 99 percent probability, and there is only only incident at a time. All incident models are equally likely. With these assumptions, the transitional probability can be constructed. In CORSIM, the left boundary condition is set as 7000veh/hour and the right

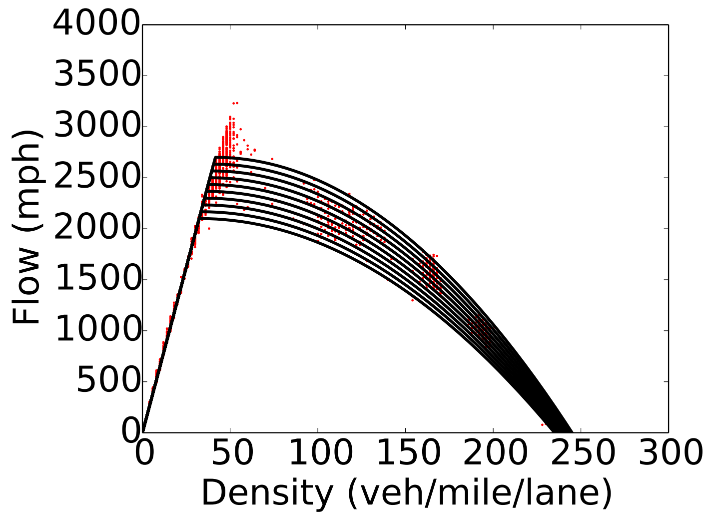

Figure 10: *Calibrated fundamental diagrm for the second order traffic flow model.*

boundary condition is set as free flow. In the estimation model, in left boundary condition is set as $6900 + \mathcal{N}(6900, 200^2)$ and the right boundary condition is also set as free flow.

The simulation results are shown in Figure 11. The three rows separately show the estimation results corresponding to GPS equipped vehicle headways of 10 seconds, 20 seconds, and 40 seconds. When the headway is 10 seconds, the estimation algorithm detects the incident with good accuracy and correctly estimates the traffic state. However, as the penetration rate decreases, the estimation accuracy also decreases. At lower penetrations, it becomes hard to correctly estimate the traffic state and detect incidents. The density estimation error of the three tests is illustrated in Figure 12.

Next, we compared the proposed algorithm to the traditional particle filter approach, where a deterministic second order traffic model without any incident dynamics is used. Figure 13 shows the estimation results when the headway between vehicles is 10 seconds. Clearly, when the traditional second order model and particle filter are used, the resulting traffic density estimate is poor, and the resulting congestion is completely missed. Adding incident dynamics to the model can significantly improve the estimation performance.

Finally, the computation time of the proposed algorithm is assessed. All simulations were performed on a Macbook pro, with 2.7 GHz Intel Core i7 processor and 4 GB memory. The

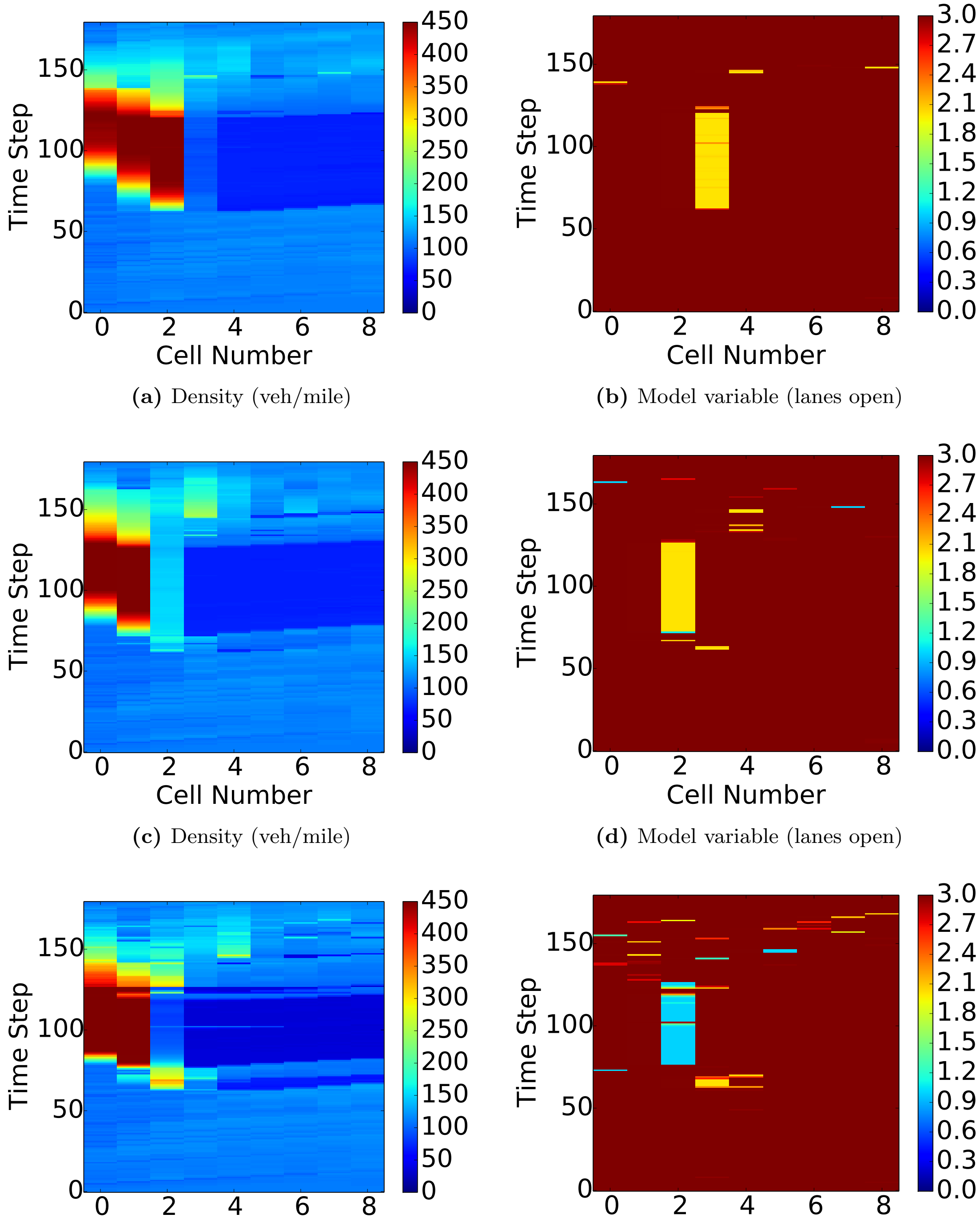

(a) Density (veh/mile) **(b)** Model variable (lanes open)

(c) Density (veh/mile) **(d)** Model variable (lanes open)

(e) Density (veh/mile) **(f)** Model variable (lanes open)

Figure 11: *Estimation results of the MMPF, probe vehicle headway 10 seconds (first row), probe vehicle headway 20 seconds (second row), probe vehicle headway 20 seconds (third row).*

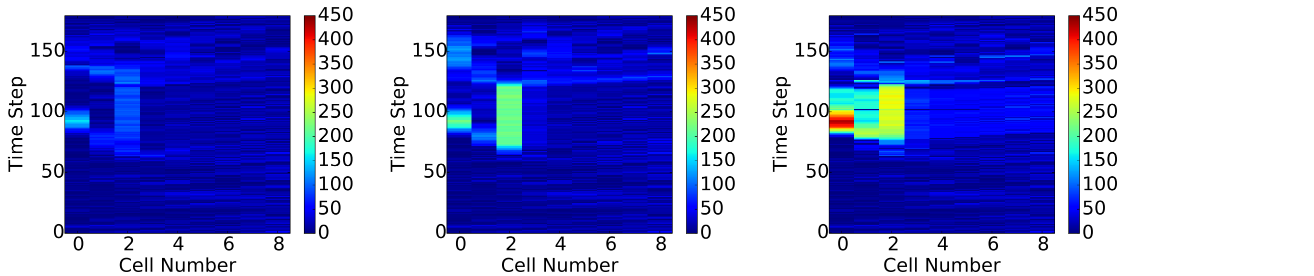

Figure 12: *Estimated density error, probe vehicle headway 10 seconds (left), probe vehicle headway 20 seconds (center), probe vehicle headway 40 seconds (right).*

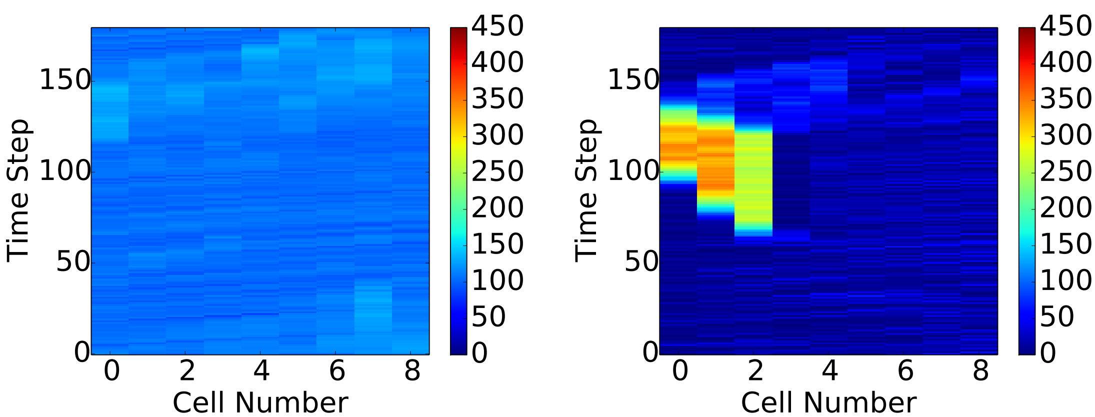

(a) Density (veh/mile)

(b) Density error (veh/mile)

Figure 13: *probe vehicle headway 10 seconds, estimated density (left), and estimation error (right).*

computation time for each of the three one-hour filtering runs is approximately 10 minutes, which is about six times faster than real–time.

3 Heterogeneous Traffic Flow Model with Creeping

3.1 Classification of Multiclass Traffic Models

Consider a system of conservation laws model of multiclass traffic flow in a general framework

$$\begin{aligned} &(\rho_j)_t + (\rho_j v_j)_x = 0, \qquad j = 1, \cdots, n, \\ &\qquad\qquad v_j = V_j(\rho), \quad \text{with} \quad \rho = (\rho_1, \cdots, \rho_n), \end{aligned} \tag{41}$$

which describes the conservation of vehicles for n vehicle classes indexed by j. Here, $\rho_j = \rho_j(x,t)$ is the traffic density of the jth class, which depends on both the location x and time t, and $V_j(\cdot)$ is the corresponding velocity function, which is a function of the density of each class. In the special case when $n = 1$, the system becomes the well-known LWR model [38, 46], and the flux function $Q(\rho) = \rho V(\rho)$ is the so-called fundamental diagram (e.g., [23, 48]). Thus, the model (41) can be interpreted as a multiclass extension of the LWR model. The existing models for multiclass traffic flow that fit into framework (41) can be classified based on their assumptions on the interaction rules of different vehicle classes characterized by the specific form of the velocity functions $V_j(\cdot)$ (see Table 1).

3.1.1 Homogeneous Multiclass Models

When all velocity functions are identical, i.e., $v_j = V(\rho)$, (41) is a *homogeneous multiclass model* since all vehicle classes follow the same kinematic behavior. These models are equivalent to the *Keyfitz–Kranzer* system [30] arising in elasticity theory. It is noted that homogeneous multiclass models are not strictly hyperbolic in general, with exceptions when $n \leq 2$ [3, 30].

An example of a homogeneous multiclass model is the *Logghe and Immers* mode [40], which relates different vehicle classes by a scaling factor known as a *passenger car equivalent*

	Model	Velocity v_j	Overtaking	Creeping
Homogeneous	Logghe & Immers [40]	$v_j = V\left(\sum_i \beta_i \rho_i\right)$	no	no
	Daganzo [15]	$v_j = V\left(\sum_i \rho_i\right)$	no	no
	Zhang & Jin [54]	$v_j = V\left(\rho_1, \rho_2\right)$	no	no
Heterogeneous	Ngoduy & Liu [45]	$v_j = V_j\left(\beta_j \sum_i \rho_i\right)$ with $v_j = V$ in congestion	freeflow	no
	Fastlane [50]	$v_j = V_j\left(\sum_i \beta_i \rho_i\right)$, with $v_j = V$ in congestion	freeflow	no
	Wong & Wong [52]	$v_j = V_j\left(\sum_i \rho_i\right)$	yes	no
	Zhu et al. [57]	$v_j = v_j^{\max} V\left(\sum_i \rho_i\right)$	yes	no
	n–populations [3]	$v_j = v_j^{\max} V\left(\sum_i \ell_i \rho_i\right)$	yes	no
	Nair et al. [44]	$v_j = pV_{\mathrm{c}}(s) + (1-p)V_{\mathrm{f}}(s)$, $p = \int_0^{s_j} g(s)ds$, $g(s)$ is distribution of s	yes	yes
	Creeping model	$v_j = V_j\left(\sum_i \ell_i \rho_i\right)$, with $V_j(0) = v^{\max}$	yes	yes

Table 1: *Classification of multiclass models according to the definition of velocity functions.*

(PCE). Accordingly, each class is modeled with a scaled fundamental diagram with a constant maximal speed, and the velocity function depends on a weighted sum of the densities of all vehicle classes called the *effective density*. Hence, the velocity function is defined as $v_j = V\left(\sum_i \beta_i \rho_i\right)$, where β_i is the PCE applied to the ith class. A similar model of this form is Daganzo's 1-pipe special lane model [15]. Moreover, Zhang and Jin's model [54] can be treated as a special case of the Keyfitz–Kranzer system with $n = 2$.

Homogeneous multiclass models with $n = 2$ are also equivalent to a class of second order models in the GOSM framework [34] when the velocity is a strictly decreasing function of ρ_1 and ρ_2 (see Section 3.2). A primary limitation of homogeneous models is that they do not allow one vehicle class to overtake another [3], which is an important feature for highly heterogeneous flows. Consequently, the GOSM cannot model creeping (i.e., overtaking when one vehicle class has stopped).

3.1.2 Heterogeneous Multiclass Models

Many research efforts are devoted to the design of *heterogeneous multiclass models* by distinguishing $V_j(\cdot)$ for each class. The model by Ngoduy and Liu [45] characterizes vehicle classes by their maximum velocities, and assumes that the freeflow velocity depends on a *PCE–scaled density*, i.e., $v_j = V_j\left(\beta_j \sum_i \rho_i\right)$, where β_j is the PCE factor of the jth class. The model uses the same velocity function for all classes in congestion. The *Fastlane* model [50] also supposes that all vehicle classes have distinct velocity functions in freeflow but the same function in congestion, however, it defines the velocity as a function of the effective density (e.g., $v_j = V_j\left(\sum_i \beta_i\rho_i\right)$). As a consequence, the Ngoduy and Liu and Fastlane models [45, 50] allow overtaking in the freeflow regime, but not in congestion.

Wong and Wong [52] introduced a simplified heterogeneous multiclass model of the form (41) that admits overtaking in freeflow and congestion. The velocity function of each class is a function of the *total density* (e.g. $v_j = V_j\left(\sum_i \rho_i\right)$) and they are distinct except at the jam density. The model of Zhu et al. [57] also follows the same principle. Later, Benzoni–Gavage and Colombo [3] introduced the *n–populations model*, which extended Wong and Wong's model [52] by explicitly taking the size of each vehicle class into account. Hence, the PCE is chosen as the average length of each vehicle class ℓ_j. Instead of explicitly conserving the number of vehicles, the system expresses conservation of the space occupied by each vehicle class. Consequently, the velocity function depends on the *total occupied space* $r = \sum_j \ell_j\rho_j$, i.e., $v_j = V_j\left(r\right)$. As presented in [3], by substituting $\hat{\rho}_j := \ell_j\rho_j$ in the n–populations model, both models [3, 52] fit into the same mathematical framework

$$\begin{aligned} \left(\hat{\rho}_j\right)_t + \left(\hat{\rho}_j v_j\right)_x = 0, \qquad j = 1, \cdots, n, \\ v_j = V_j(r), \quad \text{with} \quad r = \sum_{j=1}^{n} \hat{\rho}_j. \end{aligned} \tag{42}$$

The models [3, 52, 57] suppose all vehicle classes either never stop [52], or stop at a common *maximum occupied space* $r^{\max}$ (or equivalently an *effective jam density*), i.e., $V_j(r^{\max}) = 0$,

$j = 1, \cdots, n$. In circumstances when the vehicles are highly heterogeneous in size, this assumption may be violated. Indeed, one can observe that at a certain level of congestion, larger vehicles such as cars and buses completely stop, while smaller vehicles such as motorcycles continue to move through the gaps between the large vehicles. This *creeping* behavior can be interpreted as a special lane which can only be used by small vehicles.

A heterogeneous multiclass model that allows for creeping is proposed by Nair et al. [44], which also fits into the generic framework (42). In this model, the velocity of each vehicle class is determined by the availability of empty spaces s (pores) for which vehicles of various sizes compete. Letting s_j represent a critical pore size for the jth class, vehicles may be in freeflow ($s \geq s_j$) or congestion ($s < s_j$) with velocity functions $V_{\mathrm{f}}(\cdot)$ and $V_{\mathrm{c}}(\cdot)$, respectively. The overall velocity of the jth class is

$$v_j = V_j\left(s\right) = \left(\int_{s_j}^{\infty} g(\omega)d\omega\right) V_{\mathrm{f}}(s) + \left(\int_{0}^{s_j} g(\omega)d\omega\right) V_{\mathrm{r}}(s), \tag{43}$$

where $g(\cdot)$ is the probability density function of the pores sizes for a given time, and $V_{\mathrm{c}}(s) \leq V_{\mathrm{f}}(s)$. The creeping property is shown by numerical simulations for a flow with two vehicle classes, but significant analytical results are missing due to the complexity of the model (43), e.g., the density function $g(s)$ evolves with time. Interestingly, the model [44] reduces to homogeneous multiclass model when $V_{\mathrm{c}}(s) = V_{\mathrm{f}}(s)$.

In this study, a two class heterogeneous model that exhibits creeping is proposed. To understand the reason why second order traffic models (GOSM) are not suitable to model creeping, a connection between the GOSM and the two class homogeneous multiclass traffic model is established next.

3.2 Interpretation of the GOSM as a Two Class Homogeneous Multiclass Model

As pointed out in [4, 17, 19], the GOSM [17, 34] (3) can be interpreted as a second order generalization of the LWR model, which allows for different vehicle properties such as aggressivity

[16]. In the GOSM framework, vehicles with the property w adjust their spacing $s = 1/\rho$ for a given velocity level v, where ρ is determined such that $v = V(\rho, w)$. An aggressive driver tends to select a smaller space when traveling at the same speed as a passive driver.

Similarly, the various interaction behaviors among different classes in multiclass flow can also be interpreted as an assignment of road space to vehicle classes [41]. Hence, it is possible to link two class heterogeneous models with the ARZ model. Consider a multiclass flow that is composed of cars ($j = 1$) and trucks ($j = 2$). By letting $\rho = (\rho_1 + \rho_2)$ be the total density and defining $w = \rho_1/\rho$ as the fraction of vehicles in the first class, the second equation in (3) is simply a conservation law for the first class, i.e., $y = \rho w = \rho_1$. Note that it is equivalent to set the property as the fraction of the second vehicle class, i.e., $w = \rho_2/\rho$. Thus, the GOSM (3) becomes

$$\begin{aligned} (\rho)_t + \big(\rho V(\rho, \rho_1/\rho)\big)_x &= 0, \\ (\rho_1)_t + \big(\rho_1 V(\rho_1, \rho_1/\rho)\big)_x &= 0. \end{aligned} \tag{44}$$

By subtracting the second equation from the first one in (44), one obtains Zhang and Jin's [54] homogeneous two class model

$$\begin{aligned} (\rho_1)_t + \big(\rho_1 \tilde{V}(\rho_1, \rho_2)\big)_x &= 0, \\ (\rho_2)_t + \big(\rho_2 \tilde{V}(\rho_1, \rho_2)\big)_x &= 0, \end{aligned} \tag{45}$$

with $\tilde{V}(\rho_1, \rho_2) = V(\rho_1 + \rho_2, \rho_1/(\rho_1 + \rho_2))$. Furthermore, one verifies that the requirement $\partial_\rho V < 0$ in the GOSM is met under a sufficient condition:

$$\partial_{\rho_1} \tilde{V}(\rho_1, \rho_2) < 0, \quad \text{and} \quad \partial_{\rho_2} \tilde{V}(\rho_1, \rho_2) < 0. \tag{46}$$

Thus, the GOSM is equivalent to a two class homogeneous multiclass model of the form (45) under the condition (46). Note that $v = V(\rho, w)$, $w = \rho_1/\rho$ generates a family of velocity curves that is parametrized by the fraction of cars. As the fraction of cars increases for a fixed total density ρ, the velocity curve shifts upwards.

Based on the equivalent formulations established, one concludes that (i) similar as homogeneous multiclass models, the GOSM is not appropriate to capture creeping; and (ii) all the analytical results of the GOSM (e.g., [2, 34, 53]) transfer over to the models of the general form (45) provided the velocity function is monotonically decreasing in the total density. This completes the mathematical analysis of homogeneous two class models, e.g., the Logghe and Immers model [40]. This justifies the need for making distinctions in the velocity function among different vehicle classes in order to model overtaking behavior including creeping.

3.3 A New Heterogeneous Model with Creeping

A new two class model is proposed under the framework (42) in terms of occupied space $\hat{\rho}_j = \ell_j \rho_j$, which distinguishes $r^{\max}$ in each vehicle class. By allowing $r^{\max}$ to vary between vehicle classes, the creeping phenomenon can be captured. For notational simplicity, let ρ_j represent the occupied space of the jth class, instead of using $\hat{\rho}_j$ in (42). Hence, $r = \rho_1 + \rho_2$ is the total occupied space. Suppose that the first class represents small creeping vehicles, and the second class is composed of large vehicles.

The new model is posed as a phase transition model [6, 12, 13] that considers two phases: a *non-creeping phase* and a *creeping phase*, which are defined as follows

$$\mathcal{D}_1 = \left\{(\rho_1, \rho_2) \in \mathbb{R}^2 \mid \rho_j \geq 0,\ j = 1, 2;\ 0 < \rho_1 + \rho_2 \leq r_2^{\max}\right\},$$
$$\mathcal{D}_2 = \left\{(\rho_1, \rho_2) \in \mathbb{R}^2 \mid 0 \leq \rho_2 \leq r_2^{\max};\ r_2^{\max} \leq \rho_1 + \rho_2 \leq r_1^{\max}\right\}.$$

In $\mathcal{D}_1$, the model is a system of conservation laws, where the dynamics of both vehicle classes can be studied. In $\mathcal{D}_2$, the large vehicles are stationary at a time t, and thus the density remains unchanged, i.e., $(\rho_2)_t = 0$. In this case, the system reduces to the LWR model for ρ_1 with possibility of discontinuous fluxes in space, which correspond to shock profiles of ρ_2. Thus, $\mathcal{D}_2$ represents a creeping phase, and $\mathcal{D}_1$ is a non-creeping phase (see Figure 14(b)). The domain $\mathcal{D}$ of the model (48) is defined as a union of $\mathcal{D}_1$ and $\mathcal{D}_2$:

$$\mathcal{D} = \left\{(\rho_1, \rho_2) \in \mathbb{R}^2 \mid 0 \leq \rho_j \leq r_j^{\max},\ j = 1, 2;\ 0 < \rho_1 + \rho_2 \leq r_1^{\max}\right\}, \tag{47}$$

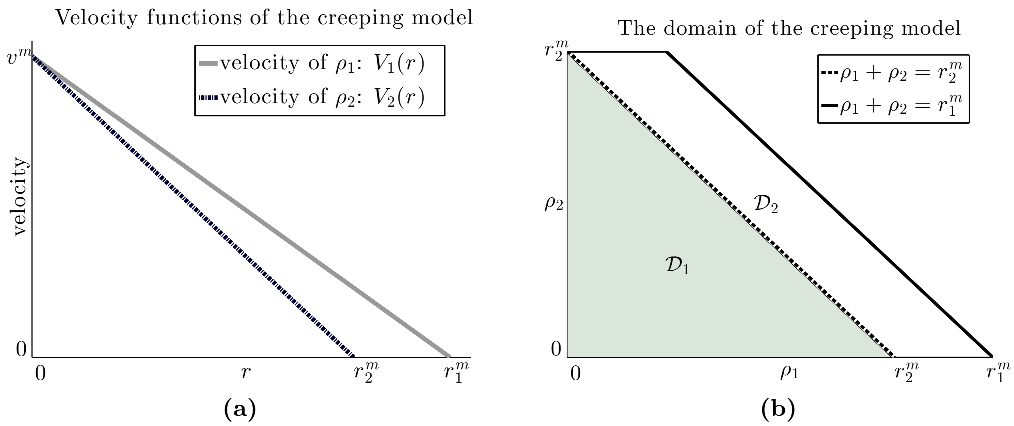

Figure 14: *(a) Velocity functions of the creeping model (51). Here, the solid-gray line represents the velocity of the first vehicle class, and the dashed-blue line is the velocity of the second vehicle class. (b) The domain of the creeping model (51).*

which has a trapezoidal shape. Note that the vacuum is excluded from $\mathcal{D}$.

The model is written as

$$\begin{cases} \begin{cases} (\rho_1)_t + \big(\rho_1 V_1(r)\big)_x &= 0, \\ (\rho_2)_t + \big(\rho_2 V_2(r)\big)_x &= 0, \end{cases} & \text{if} \ \ (\rho_1,\rho_2)\in\mathcal{D}_1, \\ \\ \begin{cases} (\rho_1)_t + \big(\rho_1 V_1(r)\big)_x &= 0, \\ \text{with} \quad (\rho_2)_t &= 0, \end{cases} & \text{if} \ \ (\rho_1,\rho_2)\in\mathcal{D}_2, \end{cases} \tag{48}$$

where a phase change is defined between $\mathcal{D}_1$ and $\mathcal{D}_2$.

Here, the velocity functions $V_j(\cdot)$, $j=1,2$ have the following properties

$$V_j'(r) < 0, \quad V_j(0) = v^{\max}, \quad V_1(r_1^{\max}) = V_2(r_2^{\max}) = 0, \quad r_2^{\max} < r_1^{\max} < 2r_2^{\max}, \tag{49}$$

where $r_j^{\max}$ are the maximum occupied spaces. Moreover, assume that the velocity functions are strictly decreasing, and both vehicle classes possess a common maximal speed $v^{\max}$ (see Figure 14(a)). The latter assumption is valid when the maximum velocities of different vehicle classes are restricted by a speed limit achievable by both classes. The condition $r_1^{\max} < 2r_2^{\max}$

is a realistic condition on the maximum occupied space that simplifies the mathematical analysis.

Remark 4. The phase transition models [6, 12, 13] apply a scalar conservation law in freeflow, and a system of conservation laws in congestion. In the creeping model (51), a scalar model is employed in the creeping phase, and a system of conservation laws is applied in the non-creeping phase.

Based on the assumptions in (49), one may propose various velocity functions to generate multiclass fundamental diagrams, such as Drake's exponential model, the smooth three-parameter model [19], or Greenshields model [23]. Note that some of these models may generate intersections between velocity curves for $r > 0$, which causes a loss of strict hyperbolicity away from the vacuum. This can be avoided depending on the choice of the free parameters in each model. For simplicity, the linear Greenshields model is used:

$$V_1(r) = v^{\max}(1 - r/r_1^{\max}), \qquad V_2(r) = v^{\max}(1 - r/r_2^{\max}). \tag{50}$$

The model (48) with Greenshields velocity functions (50) is written as

$$\left\{ \begin{array}{l} \left\{ \begin{array}{rcl} (\rho_1)_t + \left(\rho_1 v^{\max}(1 - (\rho_1 + \rho_2)/r_1^{\max})\right)_x & = & 0, \\ (\rho_2)_t + \left(\rho_2 v^{\max}(1 - (\rho_1 + \rho_2)/r_2^{\max})\right)_x & = & 0, \end{array} \right. \quad \text{if } (\rho_1, \rho_2) \in \mathcal{D}_1, \\ \\ \left\{ \begin{array}{rcl} (\rho_1)_t + \left(\rho_1 v^{\max}(1 - (\rho_1 + \rho_2)/r_1^{\max})\right)_x & = & 0, \\ \text{with} \quad (\rho_2)_t & = & 0, \end{array} \right. \quad \text{if } (\rho_1, \rho_2) \in \mathcal{D}_2. \end{array} \right. \tag{51}$$

By observing Figure 14(a), it is clear that the two velocity profiles only intersect at the vacuum. As shown later, this simplifies the analysis of the creeping model compared to intersections elsewhere in the domain. Because the velocity functions are linear, the deviation between the two velocity functions strictly increases with r. Alternative velocity functions may be considered to provide more control over the deviations and to potentially improve the predictive capabilities of the model. Moreover, one sees that the Greenshields model (50) generates a negative velocity for the second vehicle class for $r > r_2^{\max}$. The creeping model (51) successfully excludes the presence of this nonphysical negative velocity by applying a phase transition.

Remark 5. Another approach one may consider to avoid negative velocity in the second vehicle class while avoiding the need to pose the creeping model as a phase transition model is to redefine the velocity function as

$$\tilde{V}_2(r) = \begin{cases} V_2(r), & \text{if } r \leq r_2^{\max}, \\ 0, & \text{if } r_2^{\max} < r \leq r_1^{\max}. \end{cases}$$

This approach is penalized by the loss of strict hyperbolicity for $r > r_2^{\max}$.

Note that (51) also reduces to the LWR model in the sub-domain $\mathcal{D}_3 = \mathcal{D}_1 \cap \big(\{\rho_1 = 0\} \cup \{\rho_2 = 0\}\big)$, when one vehicle class is absent. Accordingly, it is natural to use an LWR model in $\mathcal{D}_3$, and to define phase transitions between $\mathcal{D}_3$ and other domains. However, this approach significantly increases the complexity in constructing Riemann solutions among different phases. Moreover, it is unnecessary since the creeping model (51) is strictly hyperbolic in $\mathcal{D}_1$, and as shown in Section 3.4.4, it is consistent with the LWR model in $\mathcal{D}_3$.

3.4 Model Analysis

The ultimate goal of the analysis is to show that (51) is well-posed in $\mathcal{D}$, and that the solution is physically meaningful. In $\mathcal{D}_2$, the creeping model is rewritten as

$$(\rho_1(x,t))_t + \big(f_1(\rho_2(x), \rho_1(x,t))\big)_x = 0, \tag{52}$$

where the flux function $f_1 = \rho_1 v^{\max}(1 - (\rho_1 + \rho_2)/r_1^{\max})$ is smooth in ρ_1 and ρ_2, and $\rho_2(x)$ is a bounded piecewise smooth function with a finite number of discontinuities. The well-posedness of a scalar conservation law model in the form of (52) is established in [26, 27]. Thus, it remains to analyze the creeping model (51) in $\mathcal{D}_1$.

In $\mathcal{D}_1$, well-posedness of a system of conservation laws is shown in a general approach that is based on constructing a solution to the Riemann problem for (51) with piecewise constant initial data

$$u(x,0) = \begin{cases} u^+, & \text{if } x > 0, \\ u^-, & \text{if } x < 0, \end{cases} \tag{53}$$

where $u^- = \left(\rho_1^-, \rho_2^-\right)$ and $u^+ = \left(\rho_1^+, \rho_2^+\right)$ are initial states. Based on the Riemann solver, the existence theory follows from Glimm's random choice method [21, 39] and the wavefront tracking algorithm [1, 8, 9]. These techniques both require a strictly hyperbolic system of conservation laws. As a result, a first and key issue is to establish the hyperbolicity of the creeping model (51) in $\mathcal{D}_1$.

3.4.1 Hyperbolicity of the Creeping Model in $\mathcal{D}_1$

The conservation laws system in $\mathcal{D}_1$ is rewritten in a compact form

$$u_t + f(u)_x = 0,$$

where $u = (\rho_1, \rho_2)$ is the vector of occupied space by class, and $f = \Big(\rho_1 V_1(r), \rho_2 V_2(r)\Big)$ is the flux function. The *Jacobian* is calculated as

$$\mathbf{A} = \partial f(u) = \begin{pmatrix} V_1 + \alpha_1 & \alpha_1 \\ \alpha_2 & V_2 + \alpha_2 \end{pmatrix}, \tag{54}$$

where $\alpha_1 = \rho_1 V_1'$, and $\alpha_2 = \rho_2 V_2'$. Strict hyperbolicity of (51) in $\mathcal{D}_1$ is established in the following lemma.

Lemma 1. *The creeping model (51) is strictly hyperbolic in $\mathcal{D}_1$.*

Proof. The model is strictly hyperbolic if and only if the Jacobian has two distinct eigenvalues.

The characteristic polynomial of $\mathbf{A}$ is:

$$P(\lambda) = \det(\mathbf{A} - \lambda \mathbf{I}) = \lambda^2 - (\kappa_1 + \kappa_2)\lambda + \kappa_1\kappa_2 - \alpha_1\alpha_2,$$

where $\kappa_j = v_j + \alpha_j$, and $\alpha_j \leq 0$, $j = 1, 2$. It is easy to see that P always has two real roots because

$$\delta = (\kappa_1 - \kappa_2)^2 + 4\alpha_1\alpha_2 \geq 0,$$

thus, the system is hyperbolic. The only possibility to lose strict hyperbolicity is when $\delta = 0$, which occurs when $\alpha_1 = 0$ and $V_1 = \kappa_2$, or $\alpha_2 = 0$ and $V_2 = \kappa_1$. These conditions hold only at the vacuum point, which does not belong to $\mathcal{D}_1$. Thus, λ_1 and λ_2 are distinct in $\mathcal{D}_1$, and the creeping model (51) is strictly hyperbolic in $\mathcal{D}_1$. □

Remark 6. Lemma 1 also holds for creeping models with velocity functions satisfying the conditions in (49).

Furthermore, the characteristic speeds of (51) in $\mathcal{D}_1$ are

$$\lambda_1 = 0.5\left(\kappa_1 + \kappa_2 - \sqrt{\delta}\right), \qquad \lambda_2 = 0.5\left(\kappa_1 + \kappa_2 + \sqrt{\delta}\right), \tag{55}$$

where $\lambda_1 < \lambda_2$. The left and right eigenvectors associated to each eigenvalue λ are

$$\ell_\lambda = \begin{pmatrix} \frac{1}{V_1 - \lambda} \\ \frac{1}{V_2 - \lambda} \end{pmatrix}, \qquad \gamma_\lambda = \begin{pmatrix} \frac{\alpha_1}{V_1 - \lambda} \\ \frac{\alpha_2}{V_2 - \lambda} \end{pmatrix}. \tag{56}$$

The next lemma establishes that the creeping model (51) is anistropic.

Lemma 2. *The characteristic speeds (55) are bounded above by the fastest vehicle class:*

$$\max\{\lambda_1, \lambda_2\} \leq \max\{V_1, V_2\}.$$

Proof. From (55) and the fact that $\alpha_j \leq 0$, $j = 1, 2$, the bound for λ_1 is given as

$$\lambda_1 \leq \min\{\kappa_1, \kappa_2\} \leq \min\{V_1, V_2\} \leq \max\{V_1, V_2\}.$$

For the second characteristic, one checks that

$$P\big(\max\{\kappa_1, \kappa_2\}\big) \leq 0, \quad \text{and} \quad P\big(\max\{V_1, V_2\}\big) \geq 0.$$

By the intermediate value theorem, the bound for λ_2 is established:

$$\max\{\kappa_1, \kappa_2\} \leq \lambda_2 \leq \max\{V_1, V_2\}. \tag{57}$$

Both λ_1 and λ_2 are bounded above by $\max\{V_1, V_2\}$. □

3.4.2 Property of the Characteristic Fields

Next, it is shown that the hyperbolic system (51) fits the Lax framework [31] in $\mathcal{D}_1$. This is crucial for the construction of solutions to the Riemann problem, since it implies that the Riemann solver consists of simple waves (or *elementary waves*). By the definition of Lax [31], one needs to check that both characteristic fields $\big(\lambda(u), \gamma_\lambda(u)\big)$ are either *genuinely nonlinear* ($\nabla\lambda(u) \cdot \gamma_\lambda(u) \neq 0$), or *linearly degenerate* ($\nabla\lambda(u) \cdot \gamma_\lambda(u) = 0$) for all u in $\mathcal{D}_1$. Here, $\nabla\lambda$ denotes the gradient of the function $\lambda(u)$. The following lemma verifies that the creeping model (51) is a Lax system in $\mathcal{D}_1$.

Lemma 3. *Both characteristic fields of (51) are genuinely nonlinear in $\mathcal{D}_1$.*

Proof. The proof follows the procedure outlined in [3]. Instead of evaluating $\nabla\lambda \cdot \gamma_\lambda$ directly, one defines $\varphi_\lambda(\gamma_\lambda)$ as

$$\varphi_\lambda(\gamma_\lambda) = \ell_\lambda \cdot \nabla^2 f(u) \cdot (\gamma_\lambda, \gamma_\lambda) = (\nabla\lambda \cdot \gamma_\lambda)(\ell_\lambda \cdot \gamma_\lambda),$$

and checks whether $\varphi_\lambda(\gamma_\lambda)$ is non zero, since $(\ell_\lambda \cdot \gamma_\lambda) \neq 0$. One calculates φ_λ as

$$\varphi_\lambda(\gamma_\lambda) = v^{\max}/r_1^{\max}(\lambda - V_2)\left(\left(\gamma_\lambda^{(1)}\right)^2 + \gamma_\lambda^{(1)}\gamma_\lambda^{(2)}\right) + v^{\max}/r_2^{\max}(\lambda - V_1)\left(\left(\gamma_\lambda^{(2)}\right)^2 + \gamma_\lambda^{(1)}\gamma_\lambda^{(2)}\right),$$

where $\gamma_\lambda^{(1)}$ and $\gamma_\lambda^{(2)}$ denote entries of the eigenvector γ_λ, i.e., $\gamma_\lambda = \left(\gamma_\lambda^{(1)}, \gamma_\lambda^{(2)}\right)$.

For the slower characteristic λ_1, it is clear that $\gamma_{\lambda_1}^{(1)}\gamma_{\lambda_1}^{(2)} \geq 0$ for the eigenvector γ_{λ_1} in (56). Moreover, from Lemma 2, one sees that $\varphi_{\lambda_1} < 0$ in $\mathcal{D}_1$. Thus, the first characteristic field is genuinely nonlinear in $\mathcal{D}_1$.

For the faster characteristic λ_2, φ_λ is rewritten as

$$\varphi_{\lambda_2}(\gamma_{\lambda_2}) = (\gamma_{\lambda_2}^{(1)} + \gamma_{\lambda_2}^{(2)})\left(v^{\max}/r_1^{\max}\gamma_{\lambda_2}^{(1)}(\lambda_2 - V_2) + v^{\max}/r_2^{\max}\gamma_{\lambda_2}^{(2)}(\lambda_2 - V_1)\right).$$

Thus, φ_{λ_2} vanishes if and only if

$$\gamma_{\lambda_2}^{(1)} + \gamma_{\lambda_2}^{(2)} = 0, \quad \text{or} \quad v^{\max}/r_1^{\max}\gamma_{\lambda_2}^{(1)}(\lambda_2 - V_2) + v^{\max}/r_2^{\max}\gamma_{\lambda_2}^{(2)}(\lambda_2 - V_1) = 0. \tag{58}$$

The first equality in (58) implies $\kappa_2 + \alpha_1 - \kappa_1 - \alpha_2 = 0$, which holds when $V_1 = V_2$. This implies that the second characteristic is genuinely nonlinear except at the point where two velocities coincide, i.e., at the vacuum.

Furthermore, the second equality of (58) gives

$$\lambda_2 = \frac{\kappa_2 V_1 + \kappa_1 V_2}{V_1 + V_2}. \tag{59}$$

Based on (57), it is clear that $\lambda_2 \geq \max\{\kappa_1, \kappa_2\}$. In contrast, (59) implies

$$\lambda_2 = \frac{\kappa_2 V_1 + \kappa_1 V_2}{V_1 + V_2} \leq \max\{\kappa_1, \kappa_2\},$$

so

$$\lambda_2 = \frac{\kappa_2 V_1 + \kappa_1 V_2}{V_1 + V_2} = \max\{\kappa_1, \kappa_2\}. \tag{60}$$

This further implies $\kappa_1 = \kappa_2$, in order for the second equality in (60) to hold. Moreover, by (55), $\lambda_2 = \max\{\kappa_1, \kappa_2\}$ implies $\alpha_1\alpha_2 = 0$. One solves for $\kappa_1 = \kappa_2$, and $\alpha_1\alpha_2 = 0$. The solution also lies at the vacuum. All together, $\varphi_{\lambda_2} = 0$ holds only at the vacuum, which is not in $\mathcal{D}_1$. Hence, the second characteristic field is also genuinely nonlinear in $\mathcal{D}_1$. $\square$

3.4.3 Elementary Waves

Lemma 3 implies that the Riemann solution of the creeping model can be constructed from shocks or rarefactions in $\mathcal{D}_1$. To construct a Riemann solver, one needs to investigate the geometries of Lax curves [31].

The Lax shock curves are computed from the *Rankine–Hogoniot* condition:

$$\sigma(u^+ - u^-) = f(u^+) - f(u^-), \tag{61}$$

where $\sigma \in \mathbb{R}$ is the speed of the shock. To obtain an admissible solution in the presence of a shock, the *Lax entropy condition* [31] should be met:

$$\lambda_j\left(u^+\right) \leq \sigma_j \leq \lambda_j\left(u^-\right), \qquad j = 1, 2, \tag{62}$$

where λ_j and σ_j are the characteristic and the shock speed of the jth family.

The Lax rarefaction curves are the integral curves of the eigenvectors. Note that one can choose various eigenvectors. For simplicity, consider those introduced in [3]:

$$\gamma_{\lambda_1} = \begin{pmatrix} \lambda_1 - \kappa_2 + \alpha_1 \\ \lambda_1 - \kappa_1 + \alpha_2 \end{pmatrix}, \qquad \gamma_{\lambda_2} = \begin{pmatrix} -\lambda_2 + \kappa_2 + \alpha_1 \\ \lambda_2 - \kappa_1 - \alpha_2 \end{pmatrix}. \tag{63}$$

By Lemma 2, one sees that

$$\gamma_{\lambda_1}^{(1)} \leq 0, \quad \gamma_{\lambda_1}^{(2)} \leq 0; \quad \gamma_{\lambda_2}^{(1)} \leq 0, \quad \gamma_{\lambda_2}^{(2)} \geq 0. \tag{64}$$

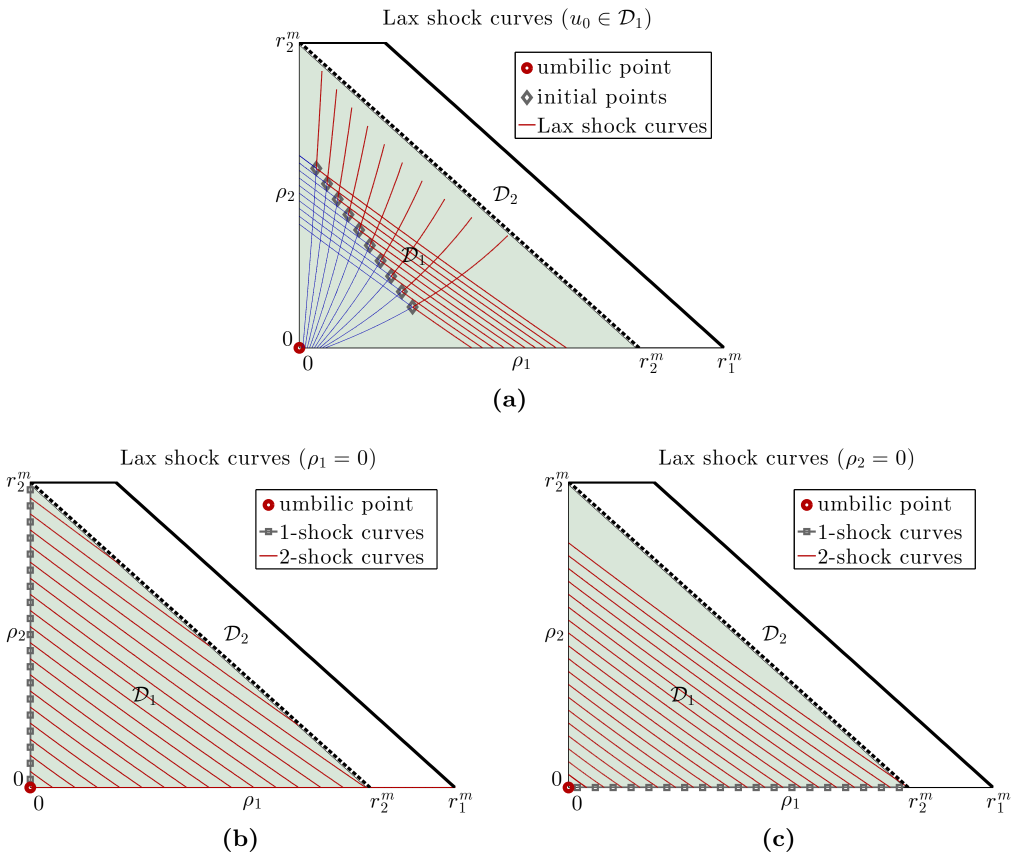

Figure 15: *Lax shock curves starting at $u_0 \in \mathcal{D}_1$. (a) illustrates the case when u_0 is interior of $\mathcal{D}_1$. (b) shows the case with u_0 on the ρ_2-axis. (c) corresponds to the case with u_0 on the ρ_1-axis. In (a), the curves with $r > \rho_1^0 + \rho_2^0$ are marked as red, and those with $r < \rho_1^0 + \rho_2^0$ are in blue color. In (b) and (c), 1–shock curves (squared-gray) remain in $\mathcal{D}_3$, and 2–shock curves (solid-red) are convex and monotonic.*

Geometry of the Lax Shock Curves From the Rankine–Hogoniot condition (61), Lax shock curves starting from an initial state $u_0 = (\rho_1^0, \rho_2^0)$ are

$$\rho_1 \left(V_1 - \sigma\right) = \rho_1^0 \left(V_1^0 - \sigma\right), \qquad \rho_2 \left(V_2 - \sigma\right) = \rho_2^0 \left(V_2^0 - \sigma\right), \tag{65}$$

where $V_1^0 = V_1 \left(\rho_1^0 + \rho_2^0\right)$ and $V_2^0 = V_2 \left(\rho_1^0 + \rho_2^0\right)$. By solving for σ in the first equation of (65), and substituting it into the second equation, (65) is rewritten as

$$\rho_2 \left((\rho_1 - \rho_1^0)V_2 - \left(\rho_1 V_1 - \rho_1^0 V_1^0\right)\right) = \rho_2^0 \left((\rho_1 - \rho_1^0)V_2 - \left(\rho_1 V_1 - \rho_1^0 V_1^0\right)\right). \tag{66}$$

Thus, Lax shock curves starting at u_0 are represented as

$$\mathcal{H}(u_0) = \left\{(\rho_1, \rho_2) \in \mathbb{R}^2 \mid \text{ s.t. (66) holds}\right\}.$$

If $u_0 \in \mathcal{D}_1 \setminus \mathcal{D}_3$, (66) is a hyperbola, which is convex and monotonic in the interior of $\mathcal{D}_1$. Moreover, 1–shock curves are strictly increasing, while 2–shock curves are strictly decreasing that exit from the ρ_1-axis (see Figure 15(a)).

When $u_0 \in \mathcal{D}_3$, e.g., on the ρ_2-axis, (66) implies either $\rho_1 = 0$, or $\sigma = V_1$. In the former case, (66) reduces to the Rankine–Hogoniot condition for an LWR model applied to the second vehicle class. This is a 1–shock curve that coincides with the ρ_2-axis. In the latter case, the shock speed is the same as the velocity of the first vehicle class $\sigma = V_1$. The hyperbola (66) for 2–shock curves becomes

$$\left(r_2^{\max} - r_1^{\max}\right) \rho_2 \left(\rho_1 + \rho_2\right) - r_2^{\max} \rho_2^0 \left(\rho_1 + \rho_2\right) + r_1^{\max} \rho_2^0 \left(\rho_1^0 + \rho_2^0\right) = 0,$$

which is convex, monotonic, and exits from the boundary $\rho_2 = 0$ (see Figure 15(b)). The analysis of the case when u_0 is on the ρ_1-axis follows the same process, in which 1–shock curves coincide with the ρ_1-axis, and 2–shock curves are convex and monotonic, which exit from the boundary $\rho_1 = 0$ (see Figure 15(c)).

Geometry of the Lax Rarefaction Curves The lemma below gives the properties for the Lax rarefaction curves.

Lemma 4. *(i) the Lax rarefaction curves of (51) defined by (63) are monotonic and convex in $\mathcal{D}_1\backslash\mathcal{D}_3$; moreover (ii) the 1–rarefaction curves are monotonically increasing, while the 2–rarefaction curves are monotonically decreasing in $\mathcal{D}_1\backslash\mathcal{D}_3$; and (iii) in $\mathcal{D}_3$, 1–rarefaction curves coincide with the ρ_1-axis and ρ_2-axis. In contrast, 2–rarefaction curves only coincide with the ρ_2-axis.*

Proof. First, the monotonicity of the Lax rarefaction curves follows from (64). To show the concavity properties of the rarefaction curves, it is noted that the curvature of an integral curve is positively proportional to $\gamma_{\lambda_j} \wedge (\nabla\gamma_{\lambda_j} \cdot \gamma_{\lambda_j})$ [3], where “ $\wedge$ ” represents the exterior product. One calculates that

$$\gamma_{\lambda_j} \wedge (\nabla\gamma_{\lambda_j} \cdot \gamma_{\lambda_j}) = \frac{2(a_1 - a_2)}{(\lambda_j - V_2)\gamma_{\lambda_j}^{(1)} + (\lambda_j - V_1)\gamma_{\lambda_j}^{(2)}}(\lambda_j - V_1)\gamma_{\lambda_j}^{(1)}\gamma_{\lambda_j}^{(2)}\left(\gamma_{\lambda_j}^{(1)} + \gamma_{\lambda_j}^{(2)}\right).$$

Here, $a_j = v^{\max}/r_j^{\max}$, and $a_1 < a_2$ by (49). Moreover, one checks that in $\mathcal{D}_1$

$$\gamma_{\lambda_j} \wedge (\nabla\gamma_{\lambda_j} \cdot \gamma_{\lambda_j}) \leq 0, \qquad j = 1, 2. \tag{67}$$

By the definition of the eigenvectors (64), one sees the curvature center of each integral curve lies above the integral curve, which implies that the rarefaction curves are convex.

Moreover, these curves have zero curvature if the equality in (67) holds:

$$\gamma_{\lambda_j}^{(1)} + \gamma_{\lambda_j}^{(2)} = 0, \quad \text{or} \quad \lambda_j = V_1, \quad \text{or} \quad \gamma_{\lambda_j}^{(1)} = 0, \quad \text{or} \quad \gamma_{\lambda_j}^{(2)} = 0. \tag{68}$$

For the 1–rarefaction curves, the conditions in (68) are equivalent to

$$\rho_1 = 0, \quad \rho_2 > 0, \quad \text{or} \quad \rho_2 = 0, \quad \rho_1 > 0.$$

In other words, 1–rarefaction curves starting from a point in $\mathcal{D}_3$ remain in $\mathcal{D}_3$.

For the 2–rarefaction curve, the equality $\lambda_2 = V_1$ in (68) gives $\rho_1 = 0,\ \rho_2 > 0$, and the other equalities in (68) are not possible for the creeping model (51) in $\mathcal{D}_1$. Thus, the 2–rarefaction curves starting from a point lying on the ρ_2-axis coincide with the ρ_2-axis. When starting from a point on the boundary $\rho_2 = 0$, the rarefaction curves are convex, monotonic, and exit the boundary $\rho_1 = 0$. □

Based on the discussion in previous sections, the properties of the Lax curves in $\mathcal{D}_1$ have been established. To assure admissible solutions, the Lax entropy condition (62) must be satisfied for shock and rarefaction solutions [3, 55]. In particular, the total occupied space r increases along a shock curve, i.e., $\rho_1^- + \rho_2^- < \rho_1^+ + \rho_2^+$. In contrast, rarefaction curves connect a higher r at the upstream to a lower one on the downstream, i.e., $\rho_1^- + \rho_2^- > \rho_1^+ + \rho_2^+$. Hence, the Lax curves that violates the entropy condition are truncated. For instance, 2–shock curves starting at the boundary $\rho_2 = 0$ connect to smaller r values (see Figure 15(c)), thus, these curves are not admissible.

The investigation of the elementary waves is completed by studying the Lax curves in the creeping phase $\mathcal{D}_2$. In this case, the creeping model reduces to an LWR model for the first vehicle class, and ρ_2 is stationary. Thus, in the ρ_2 vs. ρ_1 plane, the characteristic curves are parallel to the ρ_1-axis.

3.4.4 Riemann Solver in $\mathcal{D}$

Recall that the Riemann problem is the building block to construct a weak solution to the Cauchy problem for hyperbolic conservation laws. Due to the difficulty to obtain the *Riemann invariant* [8, 31, 32] associated with each characteristic field in heterogeneous multiclass models, it is extremely difficult to construct an explicit Riemann solver [3, 55]. Alternatively, the existence and uniqueness of a solution to the Riemann problem is established based on the existing theories. Moreover, as shown later in Section 3.5.1, the lack of an exact Riemann solver does not cause a problem in the numerical solver.

Following the standard theory for hyperbolic conservation laws, a general solution to the

Riemann problem with piecewise constant initial states (53) is defined by first connecting the left state u^- to an intermediate state u^* with curves of the first family (1–Riemann invariant is constant along 1–Lax curves), and then connecting u^* to the right state u^+ with curves of the second family (2–Riemann invariant is constant along 2–Lax curves).

When both initial states are in $\mathcal{D}_1$, one constructs a unique Riemann solution based on the structure of the Lax curves [31]. Here, it is important to verify that the solutions are physically meaningful. In $\mathcal{D}_3$, an example that gives non-physical solutions is considered in the n–populations model [3]. Given an initial condition with no vehicles of the second type, the solution to the Riemann problem produces an intermediate state (ρ_1^*, ρ_2^*) with the presence of the second class, i.e., $\rho_2^* > 0$. This is clearly incorrect because the second vehicle class appears in the solution when initially it did not exist. The correct solution should be $\rho_2^* = 0$, and the Riemann solution should be consistent with the LWR model. The issue illustrated in this example [3] is due to the loss of strict hyperbolicity in the n–populations model.

One verifies that the creeping model (51) is consistent with the LWR when only one vehicle class is present. Based on the investigations of the geometry of Lax curves in Section 3.4.3, 1–Lax curves remain in $\mathcal{D}_3$. Therefore, it is clear that Riemann solutions are consistent with those of the LWR model.

When u^- and u^+ are in $\mathcal{D}_2$, a Riemann problem for the LWR model is solved (see e.g., [36]). Thus, to complete the Riemann solver in $\mathcal{D}$, it remains to define a solution for phase transitions between $\mathcal{D}_1$ and $\mathcal{D}_2$. Consider the Riemann problem (53) with $u^- \in \mathcal{D}_2$, and $u^+ \in \mathcal{D}_1$. In order to construct a Riemann solution with phase transition, one needs to find intermediate states u^* based on the elementary waves. Thus, a Riemann solution with two intermediate states is defined:

1. A phase transition is defined by connecting $u^- = (\rho_1^-, \rho_2^-)$ to the phase boundary $\rho_1 + \rho_2 = r_2^{\max}$ along a curve that is parallel to the ρ_1-axis. It is a rarefaction curve in the conservation equation for the first vehicle class. This intermediate state can be solved explicitly as $u_1^* = (r_2^{\max} - \rho_2^-, \rho_2^-)$.

2. The second intermediate state u_2^* is constructed for a hyperbolic system with two initial states u_1^*, $u^+ \in \mathcal{D}_1$.

The construction of a Riemann solution with $u^+ \in \mathcal{D}_2$, and $u^- \in \mathcal{D}_1$ follows the same procedure.

3.4.5 Invariance of $\mathcal{D}$

To guarantee a physical Riemann solution [2], one verifies that $\mathcal{D}$ (47) is an *invariant region* for the Riemann problem. For convenience, the invariance of the two subdomains $\mathcal{D}_1$ and $\mathcal{D}_2$ is shown, and then the cases in the presence of a phase transition are considered.

First, it is easy to check that $\mathcal{D}_1$ is invariant since the creeping model (51) meets the sufficient conditions proposed by Hoff [25].

Second, the domain $\mathcal{D}_2$ is invariant. This is because the Lax curves in $\mathcal{D}_2$ are parallel to the ρ_1-axis, and thus Riemann solution remains in $\mathcal{D}_2$ given both initial states in $\mathcal{D}_2$. Finally, in the presence of a phase transition, the Riemann solution also remains in $\mathcal{D}$ (see Section 3.4.4). It is concluded that $\mathcal{D}$ is invariant.

Remark 7. The invariance of $\mathcal{D}$ excludes the appearance of an intermediate vacuum state, which exists for example in the ARZ model [2, 17].

By the Riemann solver described in Section 3.4.4, the Riemann solution always depends continuously on the initial data, even with the presence of phase transitions. Therefore, it can be verified that the size of the wave that connects two initial states $\sum(u^-, u^+)$ of a Riemann problem is bounded

$$c \cdot \|u^+ - u^-\| \leq \sum(u^-, u^+) \leq C \cdot \|u^+ - u^-\|, \tag{69}$$

where c and C are given constants.

Next, the well-posedness of the Cauchy problem for the creeping model in $\mathcal{D}$ is established.

3.4.6 Cauchy Problem

Following the theories of phase transition models in [6, 12, 13], a weak solution to the Cauchy problem of the system (51) is defined following a standard formulation. In particular, the fluxes on the left and right states are defined when there is a phase change:

$$f^- = \begin{cases} \sum_j \rho_j^- V_j(\rho_1^- + \rho_2^-), & \text{if } (\rho_1^-, \rho_2^-) \in \mathcal{D}_1 \\ \rho_1^- V_1(\rho_1^- + \rho_2^-), & \text{if } (\rho_1^-, \rho_2^-) \in \mathcal{D}_2 \end{cases},$$

$$f^+ = \begin{cases} \sum_j \rho_j^+ V_j(\rho_1^+ + \rho_2^+), & \text{if } (\rho_1^+, \rho_2^+) \in \mathcal{D}_1 \\ \rho_1^+ V_1(\rho_1^+ + \rho_2^+), & \text{if } (\rho_1^+, \rho_2^+) \in \mathcal{D}_2 \end{cases},$$

where the Rankine–Hogoniot condition (61) must be satisfied:

$$\sigma \cdot \left(\sum_j \rho_j^+ - \sum_j \rho_j^- \right) = f^+ - f^-.$$

The existence of an admissible solution to the Cauchy problem of the creeping model (51) is proved by a standard wavefront tracking procedure [1, 8, 9]. Here, a sketch of the proof is provided. Given a piecewise constant initial state with small total variation, the front tracking algorithm defines a sequence of piecewise constant approximations $(u_k)_{k>1}$ by piecing together Riemann solutions at each interface where two fronts interact for each time step. Based on (69), one sees that the total variation of $u_k(\cdot, t)$ is bounded uniformly for arbitrary initial states with small total variation. Finally, following the Glimm scheme [21, 39], one can construct a subsequence of approximation solutions that converges to a unique admissible weak solution, which depends continuously with initial data in $\mathcal{D}$.

3.4.7 Vacuum Problem

The mathematical analysis of the previous sections is restricted to $\mathcal{D}$, which excludes the vacuum. In practice, vacuum initial states are physically meaningful, e.g., the downstream of a red traffic light is empty. Thus, an appropriate model should define a solution to the

Riemann problem with an initial state or both initial states at the vacuum. The latter case is trivial: the Riemann solution remains at the vacuum. The cases with only one initial state at the vacuum are explored next.

Upstream Vacuum State One studies the Lax curves emanating from the vacuum $u_0 = (0,0)$. By the Rankine–Hogoniot condition:

$$\rho_1 = 0, \quad \sigma = V_2(\rho_2), \quad \text{or} \quad \rho_2 = 0, \quad \sigma = V_1(\rho_1).$$

These give 1–shock curves along the ρ_2-axis, and 2–shock curves along the ρ_1-axis.

Hence, in the case connecting the vacuum on the left to $u^+ \in \mathcal{D}_1$, the shock solution first connects to an intermediate state on the ρ_2-axis with a 1–shock curve that coincides with the ρ_2-axis. A physical interpretation of this case is to consider a road with a queue of both large and small vehicles at the downstream, and an empty road at the upstream. By the definition of velocity function (see Figure 14(a)), the smaller vehicles possess a higher velocity for the same total occupied space r. Thus, after a short period of time, only the larger vehicle class ρ_2 is observable at back of the queue because the first vehicle class overtakes them, i.e., $\rho_1^* = 0$ and $\rho_2^* > 0$. Therefore, starting from a vacuum state on the left, the Lax shock curves always travel along the ρ_2-axis and to connect with the slower class. Furthermore, one checks that the shock speed of the 1–shock wave is the same as that predicted by the LWR model.

Downstream Vacuum State Based on the discussion in Section 3.4.3, 1–rarefaction curves connect to the vacuum along the boundaries $\rho_1 = 0$ and $\rho_2 = 0$. Thus, the solution to the case with $u^- \in \mathcal{D}_3$ is clear, where u^- is connected with the vacuum along the boundaries $\rho_1 = 0$ and $\rho_2 = 0$. It remains to discuss the case when $u^- \in \mathcal{D}_1 \backslash \mathcal{D}_3$.

By the features of Lax rarefaction curves (see Section 3.4.3), 1–rarefaction curves are monotonic, convex, and exit from the $\rho_2 = 0$ boundary. Thus, u^- first connects to an intermediate state on the ρ_1-axis via a 1–rarefaction curve. This also has clear physical interpretation. As two vehicle classes flow into an empty road, the smaller vehicle class ρ_1 advances to the front of the traffic, since it possesses higher speed for the same total occupied space r (see Figure 14(a)). Thus, the intermediate state u^* that connects to the vacuum at the downstream contains only vehicles of the first class. Moreover, the u^* and u^+ are connected along the ρ_1-axis.

Riemann Solver at Vacuum The Riemann solver for the vacuum problem is summarized as

Case 1: u^- is at the vacuum (shock solution):

1. $\rho_1^+ > 0,\ \rho_2^+ > 0$: It is a shock solution that connects u^- to $u^* = (0, \rho_2^*)$ by a 1–shock curve along the boundary $\rho_1 = 0$, with $\rho_1^+ + \rho_2^+ > \rho_2^* > \rho_2^+$, then connects u^* and u^+ with a 2–shock curve.

2. $\rho_1^+ = 0,\ \rho_2^+ > 0$: The solution simplifies to a single 1–shock curve that connects u^- with u^+ along the ρ_2-axis.

3. $\rho_1^+ > 0,\ \rho_2^+ = 0$: The intermediate state u^* coincides with the vacuum. Hence, u^- and u^+ are connected by a 2–shock curve along the ρ_1-axis.

Case 2: u^+ is at the vacuum (rarefaction solution):

1. $\rho_1^- > 0,\ \rho_2^- > 0$: In this case, the intermediate state appears on the ρ_1-axis, i.e., $u^* = (\rho_1^*, 0)$ with $\rho_1^- + \rho_2^- > \rho_1^* > 0$. Thus, the Riemann solution first links u^- and u^* with 1–rarefaction, and then to connect u^* and the vacuum state along the ρ_1-axis.

2. $\rho_1^- = 0,\ \rho_2^- > 0$, or $\rho_1^- > 0,\ \rho_2^- = 0$: The left state u^- connects to the vacuum on the right hand side directly via 1–rarefaction curves.

Case 3: both initial states are at the vacuum: Solution remains at the vacuum.

Stability Near the Vacuum The stability of the Riemann solver with initial data near the vacuum is briefly discussed. Riemann solutions are constructed for a left state perturbed away from the vacuum, and a fixed right state.

1. u^- is perturbed to the ρ_2-axis, $\rho_1^- = 0,\ 1 \gg \rho_2^- > 0$: The Riemann solution is composed of a 1–shock curve that connects u^- to $u^* = (0, \rho_2^*)$ with $\rho_1^+ + \rho_2^+ > \rho_2^* > \rho_2^-$ along the ρ_2-axis, and then a 2–shock curve that connects u^* to u^+.

2. u^- is perturbed into the interior of $\mathcal{D}_1$, i.e., $u^- \in \mathcal{D}_1 \backslash \mathcal{D}_3$, $1 \gg \rho_1^- > 0,\ 1 \gg \rho_2^- > 0$: In this case, the 1–shock curve is slightly shifted away from the ρ_2-axis. The structure of the solver is similar to the previous case, and the deviation between these two solutions is small.

3. u^- is perturbed to the ρ_1-axis, $1 \gg \rho_1^- > 0,\ \rho_2^- = 0$: It gives an intermediate state $u^* = (\rho_1^*, 0)$ with $\rho_1^* > \rho_1^+ + \rho_2^+$. First, u^- connects to u^* along a 1–shock curve that coincides with the ρ_1-axis. Second, u^* connects to u^+ via a 2–rarefaction curve.

In the third case, the 1–shock wave has a larger amplitude than the previous two cases, and the 2–shock wave is replaced by a 2–rarefaction wave. Thus, the structure of the Riemann solution changes for a small perturbation of the Riemann data. This may result in a loss of the continuous dependence on the initial data. Consequently, it is possible to lose well-posedness when the vacuum is involved. Due to the difficulty to obtain explicit solutions to the Riemann problems, the well-posedness of the creeping model in the presence of the vacuum problem is an open question.

3.5 Numerical Simulations

3.5.1 Numerical Method

This section is devoted to illustrate the creeping model (51) in numerical simulations, using the Godunov method [22, 36]. The update rule is given explicitly as

$$\begin{pmatrix} \rho_{1,i}^{k+1} \\ \rho_{2,i}^{k+1} \end{pmatrix} = \begin{pmatrix} \rho_{1,i}^{k} \\ \rho_{2,i}^{k} \end{pmatrix} - \frac{\Delta t}{\Delta x} \left(\begin{pmatrix} (F_1)_{i+\frac{1}{2}}^k \\ (F_2)_{i+\frac{1}{2}}^k \end{pmatrix} - \begin{pmatrix} (F_1)_{i-\frac{1}{2}}^k \\ (F_2)_{i-\frac{1}{2}}^k \end{pmatrix} \right), \tag{70}$$

where Δx and Δt are sizes of the space and time step, and $\rho_{j,i}^k$ represents the density of the jth class in the ith cell at time $t = k\Delta t$. Moreover, $(F_j)_{i-\frac{1}{2}}^k$ and $(F_j)_{i+\frac{1}{2}}^k$ are numerical fluxes through the upstream and downstream boundaries of the ith cell for the jth vehicle class at time $t = k\Delta t$. These fluxes are obtained by explicitly analyzing the sending and receiving potential for each vehicle class as an analogy to the CTM [14]. In [40], a generalization of the CTM to homogeneous multiclass models is proposed. Here, a scheme for heterogeneous extension of CTM is developed.

In the CTM framework, the flow is the minimum of sending and receiving functions, where the sending function defines the number of vehicles available to be sent from upstream, and the receiving function describes the number of vehicles available to be received downstream. For simplicity, the initial states of upstream and downstream cells are represented as $u^- = (\rho_1^-, \rho_2^-)$ and $u^+ = (\rho_1^+, \rho_2^+)$. The flows of the two vehicle classes through the cell interface are determined as

$$F_1 = \min\left\{S_1(\rho_1^-, \rho_2^-),\ R_1(\rho_1^+, \rho_2^+)\right\}, \quad F_2 = \min\left\{S_2(\rho_1^-, \rho_2^-),\ R_2(\rho_1^+, \rho_2^+)\right\}, \tag{71}$$

where $S_j(\cdot)$ and $R_j(\cdot)$, $j = 1, 2$ represent the sending and receiving functions of the two vehicle classes.

Sending and Receiving Functions for ρ_1 The flux function is of the first vehicle class is defined as

$$Q_1(\rho_1, \rho_2) = \rho_1 V_1(\rho_1 + \rho_2). \tag{72}$$

The sending and receiving functions of the first vehicle class are defined as

$$S_1(\rho_1^-, \rho_2^-) = \begin{cases} Q_1(\rho_1^-, \rho_2^-), & \text{if } \rho_1^- \leq \rho_1^{\mathrm{c}}(\rho_2^-), \\ Q_1^{\max}(\rho_2^-), & \text{if } \rho_1^- > \rho_1^{\mathrm{c}}(\rho_2^-), \end{cases}$$

$$R_1(\rho_1^+, \rho_2^+) = \begin{cases} Q_1^{\max}(\rho_2^+), & \text{if } \rho_1^+ \leq \rho_1^{\mathrm{c}}(\rho_2^+), \\ Q_1(\rho_1^+, \rho_2^+), & \text{if } \rho_1^+ > \rho_1^{\mathrm{c}}(\rho_2^+), \end{cases}$$

where $Q_1^{\max}(\rho_2) = \max_{\rho_1} \{Q_1(\rho_1, \rho_2)\}$ is the maximum of (72), and $\rho_1^{\mathrm{c}}(\rho_2) = \frac{r_1^{\max} - \rho_2}{2}$ is the critical density of ρ_1 such that $Q_1^{\max}$ is obtained.

Sending and Receiving Functions for ρ_2 The second vehicle class is stationary in the creeping phase $\mathcal{D}_2$. To capture creeping, the flux function of the second vehicle class is extended in the following way

$$Q_2(\rho_1, \rho_2) = \max \{\rho_2 V_2(\rho_1 + \rho_2), 0\}.$$

The sending and receiving functions for ρ_2 become

$$S_2(\rho_1^-, \rho_2^-) = \begin{cases} Q_2(\rho_1^-, \rho_2^-), & \text{if } \rho_2^- \leq \rho_2^{\mathrm{c}}(\rho_1^-), \\ Q_2^{\max}(\rho_1^-), & \text{if } \rho_2^- > \rho_2^{\mathrm{c}}(\rho_1^-), \end{cases}$$

$$R_2(\rho_1^+, \rho_2^+) = \begin{cases} Q_2^{\max}(\rho_1^+), & \text{if } \rho_2^+ \leq \rho_2^{\mathrm{c}}(\rho_1^+), \\ Q_2(\rho_1^+, \rho_2^+), & \text{if } \rho_2^+ > \rho_2^{\mathrm{c}}(\rho_1^+), \end{cases}$$

where $Q_2^{\max}(\rho_1) = \max_{\rho_2} \{Q_2(\rho_1, \rho_2)\}$, and $\rho_2^{\mathrm{c}}(\rho_1) = \frac{r_2^{\max} - \rho_1}{2}$ is the critical density of the second vehicle class such that $Q_2^{\max}$ is obtained.

It can be shown that the numerical scheme (70) converges to the admissible weak solution of the Cauchy problem of (51). In $\mathcal{D}_1$, by checking the propagating directions of shock or rarefaction waves predicted by the model (51), the flux through each cell boundary is consistent with that predicted by the numerical scheme (71) that is based on the sending and receiving of vehicles. In $\mathcal{D}_2$, (70) collapses to the CTM [14]. Furthermore, it can be verified that the numerical solver is consistent with the creeping model with phase transitions, e.g., $F_2 = 0$, if $u^+ \in \mathcal{D}_2$.

To avoid interactions of waves from neighboring Riemann problems, the time step should satisfy the CFL condition: $v^{\max}\frac{\Delta t}{\Delta x} \leq 1$.

3.5.2 Numerical Simulations and Comparisons

Numerical simulations are performed to illustrate the properties of the creeping model, and they are compared with those of the n–populations model [3] with two vehicle classes. For these numerical tests, the following parameters for the creeping model are used:

$$v_1^{\max} = v_2^{\max} = 1.8, \quad \text{and} \quad r_1^{\max} = 1.8, \quad r_2^{\max} = 1.0.$$

In the n–populations model, let

$$v_1^{\max} = 1.8, \quad v_2^{\max} = 1.0, \quad \text{and} \quad r_1^{\max} = r_2^{\max} = 1.8.$$

Here, $v_1^{\max}$ and $v_2^{\max}$ are the maximum velocities, and $r_1^{\max}$ and $r_2^{\max}$ are the maximum effective densities of the two vehicle classes. Thus, the first vehicle class is assumed to move faster in both models. Furthermore, the computational domain is chosen as $x \in [0, 50]$, with $\Delta x = 0.05$ and the time step Δt is chosen based on the CFL condition $\Delta t = \Delta x / v^{\max}$, where $v^{\max} = \max\{v_1^{\max}, v_2^{\max}\}$.

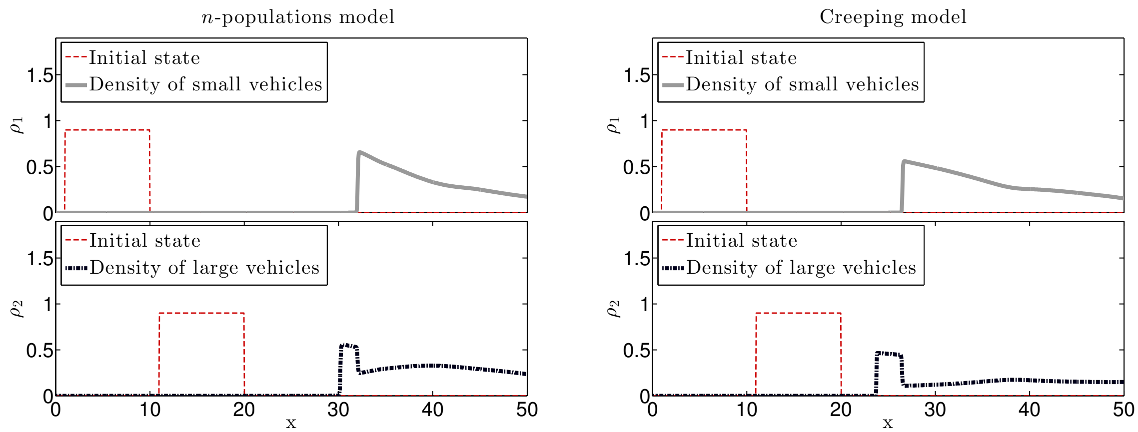

(a) **(b)**

Figure 16: *Example 1: an experiment of overtaking. (a) exhibits the traffic state of the n–populations model at $t = 50$; (b) shows the numerical results of the creeping model at $t = 33$. In each figure, the densities of the first vehicle class (thick-solid-gray) and the second vehicle class (thick-dashed-black), together with the initial condition (thin-dashed-red) are shown.*

Example 1: Overtaking In this test, the larger vehicle class ρ_2 is in front of the smaller class ρ_1 at $t = 0$. The initial condition for both vehicle classes is given as follows

$$\rho_1(x,0) = \begin{cases} 0.9, & \text{if } x \in [1,10], \\ 0, & \text{otherwise,} \end{cases} \qquad \rho_2(x,0) = \begin{cases} 0.9, & \text{if } x \in [11,20], \\ 0, & \text{otherwise.} \end{cases}$$

On the boundaries, assume the upstream inflow in zero, and vehicles are allowed to flow out of the study area freely, i.e., the downstream of the study region is empty.

As time evolves, the first vehicle class overtakes the second class. Both the n–populations model [3] and the creeping model (51) exhibit overtaking (see Figure 16), although at different time due to the structure of the two models.

Example 2: Creeping The next example depicts a scenario when two vehicle classes approach a red traffic light. Here, the same model parameters are applied as in the Example 1,

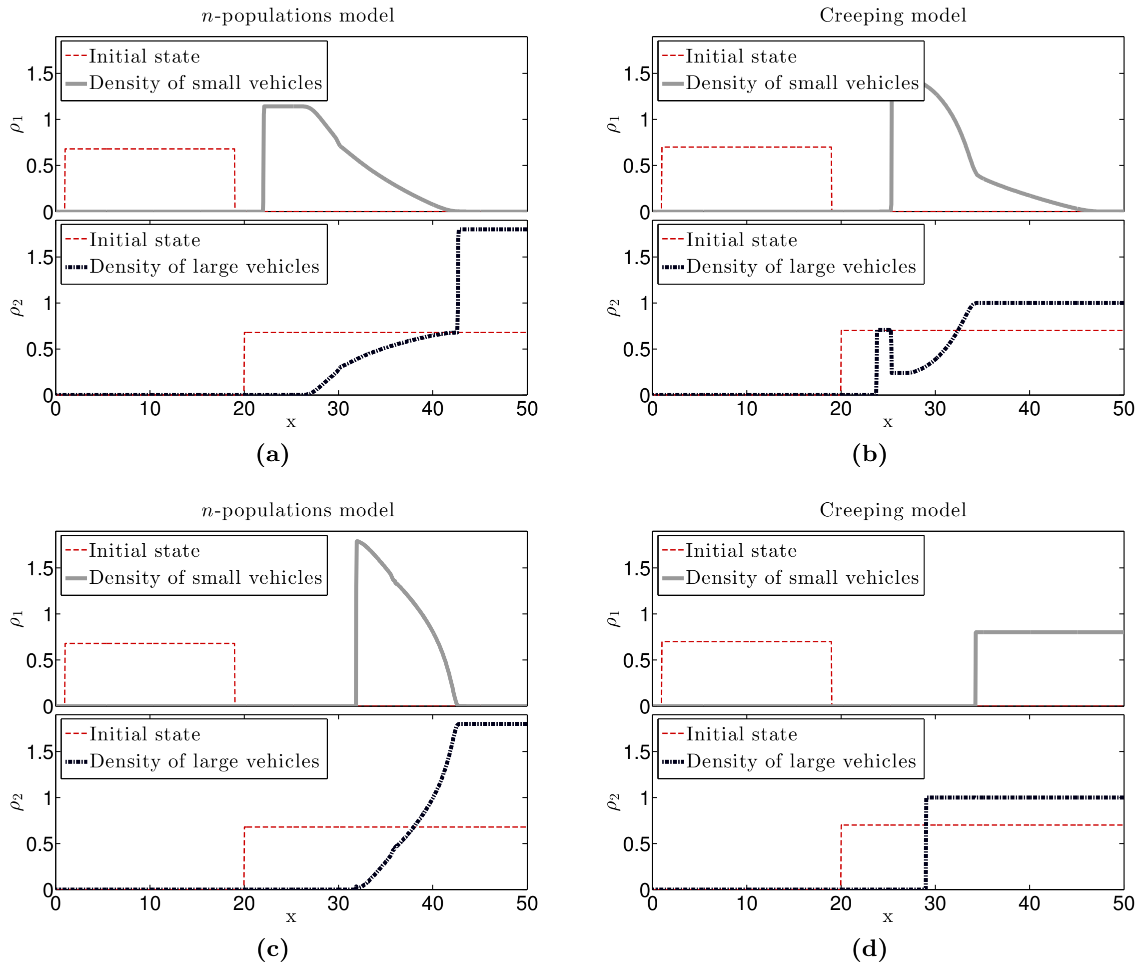

Figure 17: *Example 2: an experiment of creeping. (a) and (c) (left panel) are the simulation results of the n–populations model at $t = 33$ and $t = 150$, respectively. (b) and (d) (right panel) exhibit the results of the creeping model at $t = 33$ and $t = 150$, respectively.*

but a new initial condition is given as follows

$$\rho_1(x,0) = \begin{cases} 0.7, & \text{if } x \in [1,19], \\ 0, & \text{otherwise,} \end{cases} \qquad \rho_2(x,0) = \begin{cases} 0.7, & \text{if } x \in [20,50], \\ 0, & \text{otherwise.} \end{cases}$$

The initial condition describes the situation where the first vehicle class starts behind the second vehicle class. For the boundary condition, the inflow from upstream is zero and the downstream outflow for both vehicle classes is prescribed as zero to model a red traffic light. Example 2 is suitable to illustrate the difference between the n–populations model [3] and the creeping model (see Figure 17).

At time $t = 33$, overtaking occurs in both models (see Figures 17(a), 17(b)), where the first vehicle class catches up and competes for free spaces with the second vehicle class. For the second vehicle class, shock waves are triggered from the right boundary and travel backwards into the computational domain. One observes that the second vehicle class accumulates at the traffic light.

At $t = 150$, one sees very different configurations of the density profiles in the two models (see Figures 17(c), 17(d)). In the n–populations model, the road segment adjacent to the red traffic light $x \in [42, 50]$ is occupied exclusively by larger vehicles, while traffic on the road segment $x \in [32, 42]$ is composed by two vehicle classes. It is clear that the n–populations model does not allow creeping.

In the creeping model, the first vehicle class with smaller size is able to overtake the second vehicle class even through the larger vehicles are stationary due to the red traffic light. At $t = 150$, both vehicle classes appear near the right boundary of the study area, and the smaller vehicle class creeps up to the front of the queue. Thus, this test shows that the creeping model is appropriate to model the creeping in a heterogeneous traffic flow.

4 Conclusion

In this work, the joint traffic state estimation and incident detection problem is formulated as a hybrid state estimation problem. A second order traffic flow model with incident dynamics is implemented with a MMPF to solve the estimation problem in simulation, using traffic incident data generated from CORSIM. Compared to a particle filter applied to a second order traffic flow model with time-invariant parameters, the new algorithm can significantly improve traffic estimates while also estimating the location and severity of incidents.

Next, a new heterogeneous model for two vehicle classes is developed, which is based on the philosophy that vehicles with different sizes occupy different spaces on the roadway. The model is designed to capture the creeping scenario when large vehicles are stopped, while smaller vehicles continue to move. To achieve this goal, velocity functions are introduced that have the same maximum velocity but distinct maximum occupied spaces. The model is described as a phase transition model where a 2×2 system reduces to the LWR model as the occupied space increases above a critical point $r_2^{\max}$. A Riemann solver is defined across the phase transition. Finally, numerical tests based on finite volume Godunov scheme are performed, and comparisons between creeping model and the two class n–populations model are carried out. These tests show that the creeping model can not only describe overtaking behavior, but also model the dynamics of creeping in heterogeneous flow.

References

[1] F. Ancona and A. Marson. Existence theory by front tracking for general nonlinear hyperbolic systems. *Archive for rational mechanics and analysis*, 185(2):287–340, 2007.

[2] A. Aw and M. Rascle. Resurrection of second order models of traffic flow. *SIAM J. Appl. Math.*, 60:916–944, 2000.

[3] S. Benzoni-Gavage and R. M. Colombo. An n-populations model for traffic flow. *European Journal of Applied Mathematics*, 14(5):587–612, 2003.

[4] F. Berthelin, P. Degond, M. Delitala, and M. Rascle. A model for the formation and evolution of traffic jams. *Arch. Ration. Mech. Anal.*, 187:185–220, 2008.

[5] S. Blandin, J. Argote, A. Bayen, and D. Work. Phase transition model of non-stationary traffic flow: definition, properties and solution methods. *Transportation Research Part B*, 52(2013):31–55, 2013.

[6] S. Blandin, D. Work, P. Goatin, B. Piccoli, and A. Bayen. A general phase transition model for vehicular traffic. *SIAM J. Appl. Math.*, 71(1):107–127, 2011.

[7] A. P. Blom, Henk and Y. Bar-Shalom. The interacting multiple model algorithm for systems with markovian switching coefficients. *IEEE Transactions on Automatic Control*, 33(8):780–783, 1988.

[8] A. Bressan. *Hyperbolic systems of conservation laws – The one dimensional Cauchy problem*. Oxford University Press, Oxford, 2000.

[9] A. Bressan and R. M. Colombo. The semigroup generated by $2\times$ 2 conservation laws. *Archive for rational mechanics and analysis*, 133(1):1–75, 1995.

[10] G. Bretti, R. Natalini, and B. Piccoli. A fluid-dynamic traffic model on road networks. *Archives of Computational Methods in Engineering*, 14(2):139–172, 2007.

[11] G. M. Coclite, M. Garavello, and B. Piccoli. Traffic flow on a road network. *SIAM J. Math. Anal.*, 36(6):1862–1886, 2005.

[12] R. M. Colombo. Hyperbolic phase transitions in traffic flow. *SIAM Journal on Applied Mathematics*, 63(2):708–721, 2003.

[13] R. M. Colombo, P. Goatin, and F. S. Priuli. Global well posedness of traffic flow models with phase transitions. *Nonlinear Analysis: Theory, Methods & Applications*, 66(11):2413–2426, 2007.

[14] C. F. Daganzo. The cell transmission model: A dynamic representation of highway traffic consistent with the hydrodynamic theory. *Transportation Research Part B: Methodological*, 28(4):269–287, 1994.

[15] C. F. Daganzo. A continuum theory of traffic dynamics for freeways with special lanes. *Transportation Research Part B: Methodological*, 31(2):83–102, 1997.

[16] C. F. Daganzo. A behavioral theory of multi-lane traffic flow. part i: Long homogeneous freeway sections. *Transportation Research Part B: Methodological*, 36(2):131–158, 2002.

[17] S. Fan, M. Herty, and B. Seibold. Comparative model accuracy of a data-fitted generalized Aw-Rascle-Zhang model. *Netw. Heterog. Media*, Vol. 9, No. 2:239–268, 2014.

[18] S. Fan, B. Piccoli, and B. Seibold. A collapsed generalized Aw-Rascle-Zhang model. *SIAM J. Appl. Math.*, In process.

[19] S. Fan and B. Seibold. A comparison of data-fitted first order traffic models and their second order generalizations via trajectory and sensor data. 93rd Annual Meeting of Transportation Research Board, Washington DC, 2013. paper number 13–4853.

[20] M. Garavello and B. Piccoli. Traffic flow on a road network using the aw–rascle model. *Communications in Partial Differential Equations*, 31(2):243–275, 2006.

[21] J. Glimm. Solutions in the large for nonlinear hyperbolic systems of equations. *Communications on Pure and Applied Mathematics*, 18(4):697–715, 1965.

[22] S. K. Godunov. A difference scheme for the numerical computation of a discontinuous solution of the hydrodynamic equations. *Math. Sbornik*, 47:271–306, 1959.

[23] B. D. Greenshields. A study of traffic capacity. *Proceedings of the Highway Research Record*, 14:448–477, 1935.

[24] M. Herty and M. Rascle. Coupling conditions for a class of second order models for traffic flow. *SIAM J. Math. Anal.*, 38(2):595–616, 2006.

[25] D. Hoff. Invariant regions for systems of conservation laws. *Transactions of the American Mathematical Society*, 289(2):591–610, 1985.

[26] K. H. Karlsen, N. H. Risebro, and J. Towers. Upwind difference approximations for degenerate parabolic convection–diffusion equations with a discontinuous coefficient. *IMA J. Numer. Anal.*, 22(4):623–664, 2002.

[27] K. H. Karlsen, N. H. Risebro, and J. Towers. L1 stability for entropy solutions of nonlinear degenerate parabolic convection-diffusion equations with discontinuous coefficients. *Skr. K. Nor. Vid. Selsk*, 2003.

[28] B. S. Kerner. Experimental features of the emergence of moving jams in free traffic flow. *J. Phys. A*, 33:221–228, 2000.

[29] B. S. Kerner. *Phase transitions in traffic flow.* Traffic and Granular Flow. Springer, 2000.

[30] B. L. Keyfitz and H. C. Kranzer. A system of non-strictly hyperbolic conservation laws arising in elasticity theory. *Archive for Rational Mechanics and Analysis*, 72(3):219–241, 1980.

[31] P. D. Lax. Hyperbolic systems of conservation laws II. *Communications on Pure and Applied Mathematics*, 10(4):537–566, 1957.

[32] P. G. Le Floch. *Hyperbolic Systems of Conservation Laws: The theory of classical and nonclassical shock waves.* Birkhäuser, 2002.

[33] J. P. Lebacque. The Godunov scheme and what it means for first order traffic flow models. In *13th International Symposium on Transportation and Traffic Theory*, pages 647–677, 1996.

[34] J. P. Lebacque, S. Mammar, and H. Haj-Salem. Generic second order traffic flow modelling. In R. E. Allsop, M. G. H. Bell, and B. G. Heydecker, editors, *Transportation and Traffic Theory*, Proc. of the 17th ISTTT, pages 755–776. Elsevier, 2007.

[35] J. P. Lebacque and Salim Mammar. Second order traffic flow modeling: supply-demand analysis of the inhomogeneous riemann problem and of boundary conditions.

[36] R. J. LeVeque. *Finite volume methods for hyperbolic problems.* Cambridge University Press, 2002.

[37] X. R. Li and V. P. Jilkov. Survey of maneuvering target tracking. part v. multiple-model methods. *IEEE Transactions on Aerospace and Electronic Systems*, 41(4):1255–1321, 2005.

[38] M.J. Lighthill and G.B. Whitham. On kinematic waves II. a theory of traffic flow on long crowded roads. *Proceedings of the Royal Society of London. Series A. Mathematical and Physical Sciences*, 229(1178):317–345, 1955.

[39] T. P. Liu and T. Yang. Weak solutions of general systems of hyperbolic conservation laws. *Communications in mathematical physics*, 230(2):289–327, 2002.

[40] S. Logghe and L. H. Immers. Heterogeneous traffic flow modelling with the LWR model using passenger-car equivalents. In *Proceedings of the 10th World congress on ITS, Madrid (Spain)*, 2003.

[41] S. Logghe and L. H. Immers. Multi-class kinematic wave theory of traffic flow. *Transportation Research Part B: Methodological*, 42(6):523–541, 2008.

[42] CORSIM Users Manual. FHWA. *US Department of Transportation, Office of Safety and Traffic Operations*, 1997.

[43] Efim Mazor, Amir Averbuch, Yakov Bar-Shalom, and Joshua Dayan. Interacting multiple model methods in target tracking: a survey. *IEEE Transactions on Aerospace and Electronic Systems*, 34(1):103–123, 1998.

[44] R. Nair, H. S. Mahmassani, and E. Miller-Hooks. A porous flow approach to modeling heterogeneous traffic in disordered systems. *Transportation Research Part B: Methodological*, 45(9):1331 – 1345, 2011.

[45] D. Ngoduy and R. Liu. Multiclass first-order simulation model to explain non-linear traffic phenomena. *Physica A: Statistical Mechanics and its Applications*, 385(2):667–682, 2007.

[46] P.I. Richards. Shock waves on the highway. *Operation Research*, 4(1):42–51, 1956.

[47] B. Ristic, S. Arulampalm, and N. Gordon. *Beyond the Kalman filter: Particle filters for tracking applications*. Artech House Publishers, 2004.

[48] S. Smulders. Control of freeway traffic flow by variable speed signs. *Transportation Research Part B: Methodological*, 24(2):111 – 132, 1990.

[49] S. Tafazoli and X. Sun. Hybrid system state tracking and fault detection using particle filters. *IEEE Transactions on Control Systems Technology*, 14(6):1078–1087, 2006.

[50] J. W. C. Van Lint, S. P. Hoogendoorn, and M. Schreuder. Fastlane: New multiclass first-order traffic flow model. *Transportation Research Record: Journal of the Transportation Research Board*, 2088(1):177–187, 2008.

[51] R. Wang, D. B. Work, and R. Sowers. Multiple model particle smoothing for traffic incident detection. *Submitted to IEEE Transactions on Intelligent Transportation Systems*, 2004.

[52] G. C. K. Wong and S. C. Wong. A multi-class traffic flow model an extension of LWR model with heterogeneous drivers. *Transportation Research Part A: Policy and Practice*, 36(9):827 – 841, 2002.

[53] H. M. Zhang. A non-equilibrium traffic model devoid of gas-like behavior. *Transp. Res. B*, 36:275–290, 2002.

[54] H. M. Zhang and W. L. Jin. Kinematic wave traffic flow model for mixed traffic. *Transportation Research Record: Journal of the Transportation Research Board*, 1802(1):197–204, 2002.

[55] P. Zhang, R. X. Liu, S. C. Wong, and S. Q. Dai. Hyperbolicity and kinematic waves of a class of multi-population partial differential equations. *European Journal of Applied Mathematics*, 17(2):171–200, 2006.

[56] P. Zhang, S. C. Wong, and S. Q. Dai. A conserved higher-order anisotropic traffic flow model: description of equilibrium and non-equilibrium flows. *Transportation Research Part B: Methodological*, 43(5):562–574, 2009.

[57] Z. Zhu and T. Wu. Two-phase fluids model for freeway traffic flow and its application to simulate evolution of solitons in traffic. *Journal of transportation engineering*, 129(1):51–56, 2002.